



**Air Gun Launch Simulation Modeling and Finite
Element Model Sensitivity Analysis**

by Mostafiz R. Chowdhury and Ala Tabiei

ARL-TR-3703

January 2006

NOTICES

Disclaimers

The findings in this report are not to be construed as an official Department of the Army position unless so designated by other authorized documents.

Citation of manufacturer's or trade names does not constitute an official endorsement or approval of the use thereof.

DESTRUCTION NOTICE—Destroy this report when it is no longer needed. Do not return it to the originator.

Army Research Laboratory

Adelphi, MD 20783-1145

ARL-TR-3703

January 2006

Air Gun Launch Simulation Modeling and Finite Element Model Sensitivity Analysis

Mostafiz R. Chowdhury
Weapons and Materials Research Directorate, ARL

Ala Tabiei
Private Contractor

REPORT DOCUMENTATION PAGE			<i>Form Approved</i> OMB No. 0704-0188		
Public reporting burden for this collection of information is estimated to average 1 hour per response, including the time for reviewing instructions, searching existing data sources, gathering and maintaining the data needed, and completing and reviewing the collection information. Send comments regarding this burden estimate or any other aspect of this collection of information, including suggestions for reducing the burden, to Department of Defense, Washington Headquarters Services, Directorate for Information Operations and Reports (0704-0188), 1215 Jefferson Davis Highway, Suite 1204, Arlington, VA 22202-4302. Respondents should be aware that notwithstanding any other provision of law, no person shall be subject to any penalty for failing to comply with a collection of information if it does not display a currently valid OMB control number. PLEASE DO NOT RETURN YOUR FORM TO THE ABOVE ADDRESS.					
1. REPORT DATE (DD-MM-YYYY) January 2006		2. REPORT TYPE Final		3. DATES COVERED (From - To) May to December 2003	
4. TITLE AND SUBTITLE Air Gun Launch Simulation Modeling and Finite Element Model Sensitivity Analysis			5a. CONTRACT NUMBER		
			5b. GRANT NUMBER		
			5c. PROGRAM ELEMENT NUMBER		
6. AUTHOR(S) Mostafiz R. Chowdhury (ARL); Ala Tabiei (private contractor)			5d. PROJECT NUMBER 622618H80		
			5e. TASK NUMBER		
			5f. WORK UNIT NUMBER		
7. PERFORMING ORGANIZATION NAME(S) AND ADDRESS(ES) U.S. Army Research Laboratory Weapons & Materials Research Directorate Adelphi, MD 20783-1197			8. PERFORMING ORGANIZATION REPORT NUMBER ARL-TR-3703		
9. SPONSORING/MONITORING AGENCY NAME(S) AND ADDRESS(ES)			10. SPONSOR/MONITOR'S ACRONYM(S)		
			11. SPONSOR/MONITOR'S REPORT NUMBER(S)		
12. DISTRIBUTION/AVAILABILITY STATEMENT Approved for public release; distribution is unlimited.					
13. SUPPLEMENTARY NOTES					
14. ABSTRACT <p>This report presents in two parts analytical simulation results of a test item launched in an air gun test. The first part of the report presents a discrete mass-spring model to predict the transient response of a generic artillery component subjected to launch simulation in an air gun test environment. A 2-degree-of-freedom model is developed to simulate the air gun launch environment in which a test object mounted on a projectile is launched through the air gun and decelerated by a crushing aluminum honeycomb mitigator. The mitigator in turn impacts the momentum exchange mass (MEM) before being stopped at the retrieving end. The present model achieved a good prediction of the period and peak acceleration of the on-board recorder. The sensitivity of finite element (FE) model parameters affecting the dynamics of a test object launched in an air gun test is discussed in the second part of the report. An LS-DYNA¹ FE model previously developed to simulate the impact mitigation environment is used to investigate the sensitivity of FE model parameters. The sensitivity study clearly indicates the necessity of honeycomb material characterization under very high impact loading for effective modeling of the strain rate effects. The FE analysis also suggests that intermittent eigenvalue analyses during an impact simulation could be useful in identifying the dominant modes of vibration governing the dynamics of the test items and verifying the predictive capability of the FE model. An efficient procedure using a decoupled model is proposed to simulate the response of a test item launched in an air gun test. In this approach, the contact force generated from the discrete analytical model is applied on a detailed FE mesh of the test item for a given impact velocity. The acceleration data obtained with this procedure compared well with those predicted from the full FE analysis. The simplified model runs in less than 1 minute.</p> <p>¹LS-DYNA, which is not an acronym, is a trademark of Livermore Software Technology Corp.</p>					
15. SUBJECT TERMS air gun launch simulation; aluminum honeycomb; analytical simulation; discrete spring-mass model; sensitivity					
16. SECURITY CLASSIFICATION OF:			17. LIMITATION OF ABSTRACT SAR	18. NUMBER OF PAGES 65	19a. NAME OF RESPONSIBLE PERSON Mostafiz Chowdhury
a. REPORT Unclassified	b. ABSTRACT Unclassified	c. THIS PAGE Unclassified			19b. TELEPHONE NUMBER (Include area code) 301-394-6308

Contents

List of Figures	iv
Acknowledgments	vii
1. Part I: Air Gun Modeling	1
1.1 Introduction	1
1.2 Model Formulation.....	2
1.2.1 Assumptions	2
1.2.2 Rigid Body Dynamics System	2
1.3 System Parameters Definition	5
1.3.1 OBR and MEM	5
1.3.2 Mitigator	5
1.3.3 Strain Rate Effects.....	8
1.4 Results and Discussion.....	9
1.4.1 Validation of Present Model.....	9
1.5 Parameter Variation Sensitivity.....	16
1.6 Conclusion.....	19
2. Part II: Air Gun Finite Element Simulation	20
2.1 Review of Previous Work	20
2.2 Finite Element Model Sensitivity Study	21
2.2.1 Double Versus Single Precision Code.....	21
2.2.2 Time Step Size Effect.....	23
2.2.3 Different Output Intervals	24
2.2.4 All Damping Options in LS-DYNA Investigated	25
2.2.5 The OBR Filled With Solid Elements to Represent Beads	28
2.2.6 Intermittent Eigenvalues Analysis.....	29
2.3 Simplified Simulation	31
2.4 Conclusion.....	32
3. References	34
Appendix A. Program I/O Files and FORTRAN Source Code	35
Distribution List	42

List of Figures

Figure 1. Schematic of the air gun.....	1
Figure 2. Dynamic system representation.....	3
Figure 3. Honeycomb stress-strain curve.....	6
Figure 4. Plastic shock wave.....	6
Figure 5. Mitigator deformation.	7
Figure 6. Mitigator wedge deformation zones.....	7
Figure 7. Top acceleration of the OBR unfiltered.	10
Figure 8. Top acceleration of the OBR filtered at 7000 Hz.....	11
Figure 9. Top acceleration of the OBR filtered at 2500 Hz.....	11
Figure 10. Top acceleration of the OBR filtered at 1000 Hz.....	12
Figure 11. Fast Fourier transform (FFT) of the top acceleration of the OBR.	12
Figure 12. Top velocity of the OBR.	13
Figure 13. Top displacement of the OBR.	14
Figure 14. Mitigator contact forces.....	14
Figure 15. Mitigator contact force impulse.....	15
Figure 16. Length of mitigator plastic region.	15
Figure 17. $m_1:m_2$ mass ratio sensitivity of model.....	16
Figure 18. Model sensitivity to 10% variation of the value of k_1	17
Figure 19. Model sensitivity to large variation of the value of k_1	17
Figure 20. Model sensitivity to variation of the solution time step.	18
Figure 21. Model sensitivity to 10% variation of the value of mitigator radius.....	19
Figure 22. Acceleration data for the same FE model with two different precisions.	22
Figure 23. FFT of the acceleration data.	22
Figure 24. Acceleration data for different integration time steps.....	23
Figure 25. FFT of the acceleration data for different integration time steps.	23
Figure 26. Acceleration data sampled at different frequencies.....	24
Figure 27. FFT of the acceleration data sampled at different frequencies.....	24
Figure 28. Acceleration data for simulation with mass proportional damping.....	25
Figure 29. FFT of the acceleration data for simulation with mass proportional damping.....	25
Figure 30. Acceleration data for simulation and test with mass proportional damping.	26
Figure 32. FFT of the acceleration data for simulation with stiffness proportional damping.	27
Figure 33. Acceleration data for simulation and test with stiffness proportional damping.	27
Figure 34. FFT of the acceleration data for simulation and test with stiffness proportional damping.....	28
Figure 35. Acceleration data for simulation with filled OBR.....	28
Figure 36. FFT of the acceleration data for simulation	29

Figure 37. Mode shapes for a fundamental frequency.....	30
Figure 38. Contact force between the OBR and the mitigator.....	31
Figure 39. Acceleration data of the simplified and full model.	32

INTENTIONALLY LEFT BLANK

Acknowledgments

The analytical work presented here was accomplished under a contract (Contract No. DAAD19-02-D-001, TCN: 03-054) with the Scientific Services Program of U.S. Army Research Office, Research Triangle Park, North Carolina. Air gun tests were conducted by Mr. Ara Abrahamian of the Weapons and Materials Research Directorate, U.S. Army Research Laboratory (ARL). The contributions of Mr. Ara Abrahamian, Mr. Edward Szymanski, and Mr. William McIntosh of ARL in delivering the air gun test are greatly appreciated. Dr. Dave Hampton of the U.S. Military Academy at West Point provided a helpful review of the report, which is greatly appreciated.

INTENTIONALLY LEFT BLANK

1. Part I: Air Gun Modeling

1.1 Introduction

In an air gun test, it is critical to identify the characteristics of the test environment such as the dynamic/physical properties of momentum exchange mass (MEM) and mitigator combinations in order to obtain a target forcing function. Figure 1a depicts a schematic of the air gun test setup. The test setup consists of an air gun, a pressure tube, a catch tube, and a MEM. The test item, which is placed inside the pressure tube, is launched to impact an aluminum honeycomb mitigator. The test item contains an on-board recorder (OBR) that records responses during launch simulation. The OBR case, which is hereafter referred to as the “OBR,” is shown in figure 1b with several accelerometers and strain gauges. The model developed in this study will be used to determine the response behavior of the test item mounted on a given projectile during a launch simulation air gun test. This methodology requires the development of a predictive model of responses of the test article. An analytical model is herein developed to simulate an air gun launch environment in which a test object mounted on a projectile is launched through the air gun and decelerated by the crushing of an aluminum honeycomb mitigator that impacts the MEM before being stopped at the retrieving end.



a. schematic of air gun test setup.



b. The OBR with test item.

Figure 1. Schematic of the air gun.

The objective of this effort is to develop an overall analytical model to predict the transient response of a generic artillery component subjected to launch simulation. The simulation is achieved via impact mitigation techniques whereby the component is propelled to a target inside a 4-inch carrier equipped to measure component response during the simulation. A detailed description of the developed formulation is presented in the next section.

1.2 Model Formulation

1.2.1 Assumptions

To model the response of the OBR-mitigator-MEM system during impact, an analytical model is herein developed. The model provides a closed form solution to the dynamic system driven by the central difference equations and is based on the following assumptions:

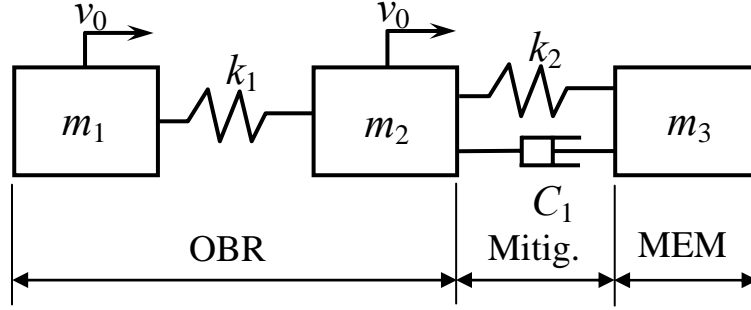
The OBR and MEM can be accurately represented by rigid bodies since they do not dissipate energy through plastic deformation. Only the lowest natural frequency of the OBR is of interest when we are predicting the acceleration output; therefore, the OBR is represented by a 2-degree-of-freedom spring-mass system. It is assumed that this frequency is readily available (if not, it can be easily determined through simple analysis).

The mass of the mitigator is neglected. The mitigator is entirely represented by the force it exerts on the OBR and the MEM. This force is determined from the geometric and material properties of the mitigator and from balance and conservation considerations during the analysis stage.

1.2.2 Rigid Body Dynamics System

The impact event is represented by a rigid body mass-spring system with 3 degrees of freedom acting along the horizontal axis. The system consists of three masses and one spring, as illustrated in figure 2. The OBR has initial velocity v_0 and is represented by two of the masses, m_1 and m_2 , and a connecting spring, k_1 . The mitigator is represented by the force F , and the MEM is represented by its mass m_3 . Note that the whole system is divided into two separate systems coupled by the force F representing the mitigator.

This assembly is a very simple representation of a complex deforming system. If the first OBR frequency mode is to be neglected, we can further simplify it by combining masses m_1 and m_2 into a single body of mass $m_{OBR} = m_1 + m_2$ and dropping spring k_1 . This will result in a 2-degree-of-freedom system. However, the essential part of this system formulation is the representation of the mitigator with the force F . To accurately represent the behavior of the mitigator, an elaborate and efficient formulation needs to be developed. Such a formulation is described in detail as follows. This simple dynamic system representation is accurate, efficient, and provides adequate results.



The system above is equivalent to the system below

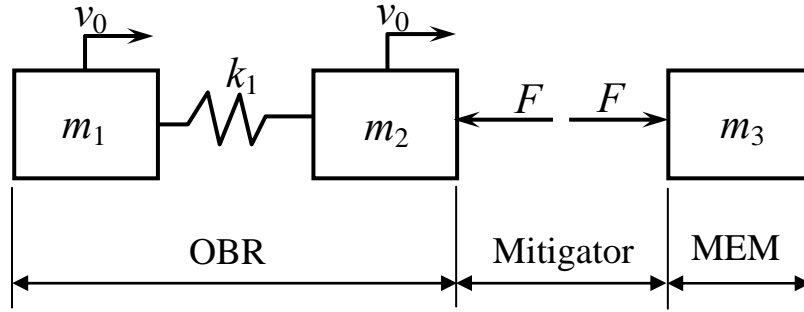


Figure 2. Dynamic system representation.

First, let us describe a time-stepping scheme to solve the dynamic system. The system's motion can be represented by the system of equations:

$$[\mathbf{M}]\{\ddot{\mathbf{u}}\} + [\mathbf{K}]\{\mathbf{u}\} = \{\mathbf{f}\} \quad (1)$$

in which

$$[\mathbf{M}] = \begin{bmatrix} m_1 & 0 \\ 0 & m_2 \end{bmatrix} \text{ is the mass matrix of the left-hand side system,}$$

$$[\mathbf{K}] = \begin{bmatrix} k_1 & -k_1 \\ -k_1 & k_1 \end{bmatrix} \text{ is the stiffness matrix of the left-hand side system,}$$

$$\{\mathbf{u}\} = \begin{Bmatrix} u_1 \\ u_2 \end{Bmatrix} \text{ is the displacement vector with } u_i \text{ being the displacement of mass } m_i$$

where $i = 1, 2$; $\{\dot{\mathbf{u}}\}$ and $\{\ddot{\mathbf{u}}\}$ are the mass velocities and accelerations, respectively.

$$\{\mathbf{f}\} = \begin{Bmatrix} 0 \\ -F \end{Bmatrix} \text{ is the external force vector.}$$

To solve this system, we define a central difference time-stepping scheme. At the initial moment ($t = 0$), we have

$$\{\mathbf{u}\}_{t=0} = \begin{Bmatrix} 0 \\ 0 \end{Bmatrix},$$

$$\{\dot{\mathbf{u}}\}_{t=0} = \begin{Bmatrix} v_0 \\ v_0 \end{Bmatrix},$$

$$\{\ddot{\mathbf{u}}\}_{t=0} = [\mathbf{M}]^{-1}(\{\mathbf{f}\}_{t=0} - [\mathbf{K}]\{\mathbf{u}\}_{t=0}) = \frac{-F_0}{m_2} \begin{Bmatrix} 0 \\ 1 \end{Bmatrix} = \begin{Bmatrix} 0 \\ 0 \end{Bmatrix}$$

To define the central difference time-stepping scheme, we expand $\{\mathbf{u}\}_{n+1}$ and $\{\mathbf{u}\}_{n-1}$ about $\{\mathbf{u}\}_n$ using a Taylor series as follows:

$$\begin{aligned} \{\mathbf{u}\}_{n+1} &= \{\mathbf{u}\}_n + \Delta t \{\dot{\mathbf{u}}\}_n + \frac{\Delta t^2}{2} \{\ddot{\mathbf{u}}\}_n + O(\Delta t^3) \\ \{\mathbf{u}\}_{n-1} &= \{\mathbf{u}\}_n - \Delta t \{\dot{\mathbf{u}}\}_n + \frac{\Delta t^2}{2} \{\ddot{\mathbf{u}}\}_n - O(\Delta t^3) \end{aligned} \quad (2)$$

in which Δt is the central difference time step and $O(\Delta t^3)$ represents additional terms of the order of Δt^3 considered negligible. Then, from equation 2 we have

$$\begin{aligned} \{\dot{\mathbf{u}}\}_n &= \frac{1}{2\Delta t} (\{\mathbf{u}\}_{n+1} - \{\mathbf{u}\}_{n-1}) \\ \{\ddot{\mathbf{u}}\}_n &= \frac{1}{\Delta t^2} (\{\mathbf{u}\}_{n+1} - 2\{\mathbf{u}\}_n + \{\mathbf{u}\}_{n-1}) \end{aligned} \quad (3)$$

Now, from the equation of motion, equation 1, it follows:

$$\begin{aligned} \left(\frac{1}{\Delta t^2} [\mathbf{M}] \right) \{\mathbf{u}\}_{n+1} &= \{\mathbf{f}\}_n - [\mathbf{K}]\{\mathbf{u}\}_n + \frac{1}{\Delta t^2} [\mathbf{M}](2\{\mathbf{u}\}_n - \{\mathbf{u}\}_{n-1}) \\ \text{or} \quad \{\mathbf{u}\}_{n+1} &= 2\{\mathbf{u}\}_n - \{\mathbf{u}\}_{n-1} + [\mathbf{M}]^{-1}(\{\mathbf{f}\}_n - [\mathbf{K}]\{\mathbf{u}\}_n) \end{aligned} \quad (4)$$

in which

$$[\tilde{\mathbf{M}}] = \frac{1}{\Delta t^2} [\mathbf{M}]$$

Equations 4 and 3 are sufficient to define a forward time-stepping scheme, provided that a sufficiently small time step, Δt , is used. To start the time-stepping scheme, $\{\mathbf{u}\}_{-1}$ needs to be available, which can be determined from the second equation of equation 2:

$$\{\mathbf{u}\}_{-1} = \{\mathbf{u}\}_0 - \Delta t \{\dot{\mathbf{u}}\}_0 + \frac{\Delta t^2}{2} \{\ddot{\mathbf{u}}\}_0$$

For the right-hand side system representing the MEM we have

$$m_3 \ddot{u}_3 = F$$

$$\frac{m_3}{\Delta t^2} ((u_3)_{n+1} - 2(u_3)_n + (u_3)_{n-1}) = F_n$$

$$(u_3)_{n+1} = \frac{\Delta t^2 F_n}{m_3} + 2(u_3)_n - (u_3)_{n-1}$$

and the velocity and acceleration of the MEM can be calculated from equation 3.

1.3 System Parameters Definition

1.3.1 OBR and MEM

The simplest part of the system (figure 2) is the MEM, which is represented by its mass only. The OBR is represented by two masses and a connecting spring. The sum of the two masses is equal to the total mass of the actual OBR. In the determination of the way in which the total mass is distributed between m_1 and m_2 , different values were used for the investigated system. It was determined that a ratio of $m_1:m_2$ anywhere from 1:2 to 2:1 gives reasonable results for the second mode or lowest fundamental frequency of the OBR (the first mode is a rigid body mode). The spring stiffness (k_1) is determined so that the frequency of the second mode is matched.

$$k_1 = \frac{\omega^2 (m_1 + m_2)}{4} \quad (5)$$

Equation 5 is derived from $|K - \omega^2 M| = 0$, for $m_1 = m_2 = m$, in which ω is the angular frequency to be matched in the model. If the value of ω is not readily available, it can be easily determined by simple testing.

1.3.2 Mitigator

The representation of the mitigator is vital to the accuracy of the simulation. In this development, it is assumed that the mitigator is built of honeycomb and consists of one continuous piece of honeycomb structure. It has one cylindrical section and one wedge-shaped part with a varying cross section on the side (see figure 1a) that is being impacted by the OBR. A typical orthotropic crush model behavior for the honeycomb material is composed of three phases as shown in figure 3 (I). These three phases include linear elastic loading, volumetric crush, and hardening to full compaction. The initial linear elastic loading phase can be represented by an elastic modulus E_e , yield stress and strain σ_y and ε_y , respectively. The volumetric crush behavior of the honeycomb material model (up to compaction strain), ε_c , is assumed to be linear, as indicated in figure 3b. The fluctuation in volumetric strain relations observed in tests (see figure 3a) is believed to have resulted from unstable buckling of honeycomb cells. The hardening phase is assumed to have a linear relation during compaction with modulus E_c . To model the mitigator, the relation between the contact force and the mitigator front deformation and their progress in time is established.

Here, it is assumed that as the wedge section deforms, it takes the shape of a truncated wedge, as was indicated by the finite element analysis (FEA) results. It is also assumed that within the wedge part, the cross-sectional area varies linearly over the wedge height. In the development of this mitigator deformation model, its mass is herein neglected; its mass and velocity throughout the event are small compared to the other moving parts. The mitigator deformation is driven in time by its elastic and plastic wave propagation speeds. Since the elastic propagation speed is much higher than the velocities in the event, it is assumed that elasticity-driven events propagate with infinite speed. Therefore, before the stress-strain state attains material yielding, it must be homogeneous along the cylinder axis.

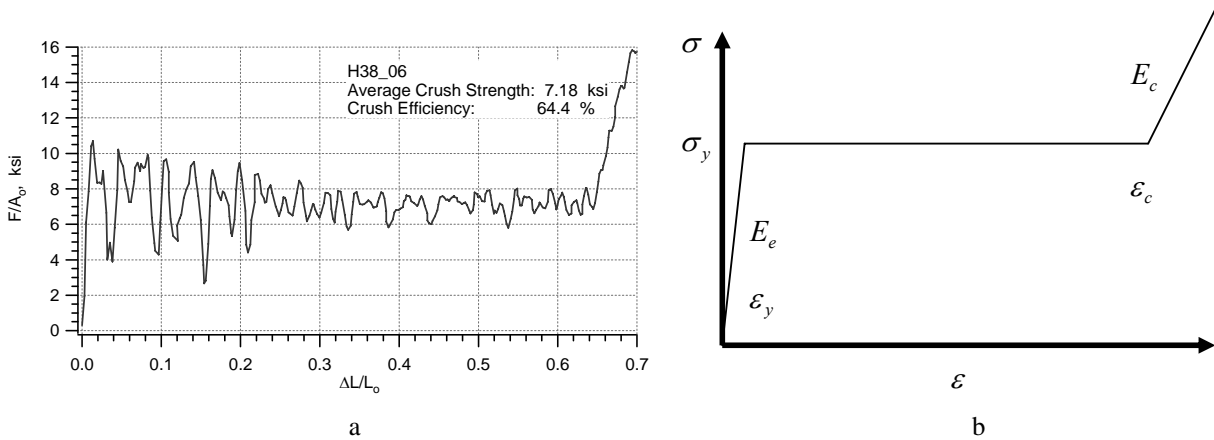


Figure 3. Honeycomb stress-strain curve.

Our aim is to determine the force resulting from the mitigator deformation within the central difference time-stepping scheme. Assuming that we have found a solution at time equal to t_n , we need to express the force at time $t_{n+1} = t_n + \Delta t$.

When the OBR hits the mitigator, a plastic region forms immediately at the wedge top. As indicated in figure 4, the boundary between this plastic region and the rest of the mitigator, which is still elastic, would travel down the length of the mitigator with variable velocity equal to the current plastic wave speed, c_{pl} (2, 3). Figure 4 also shows the respective material states (density [ρ], stress [σ]) of the crushed and elastic parts of the mitigator. The stresses, velocities, and densities on both sides of the plastic wave front are further explained in figure 5. With the approach suggested in (2) and (3), the plastic wave speed can be determined as follows.

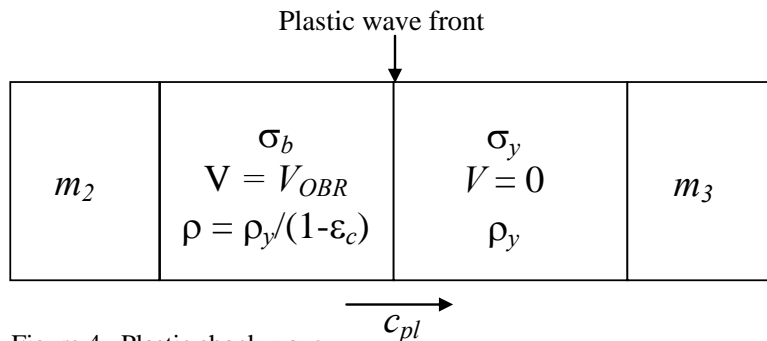


Figure 4. Plastic shock wave.

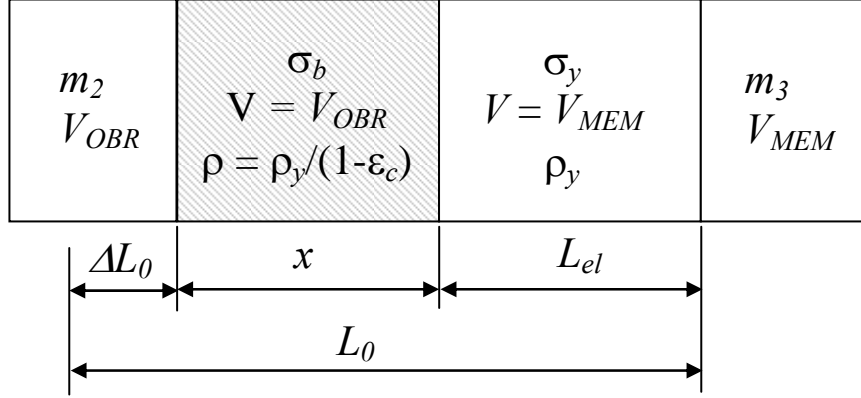


Figure 5. Mitigator deformation.

Following the notation of figure 5, let the initial length of the mitigator be L_0 . At the current analysis time, t , the total deformation of the mitigator is ΔL_0 and the lengths of the crushed and the elastic parts are x and L_{el} , respectively. Since the yield strain of the mitigator is negligible compared to its compaction strain, we can assume that all mitigator deformation, ΔL_0 , occurs in the compacted region:

$$\varepsilon_c = \frac{\Delta L_0}{x + \Delta L_0} \quad (6)$$

or

$$x = \frac{1 - \varepsilon_c}{\varepsilon_c} \Delta L_0$$

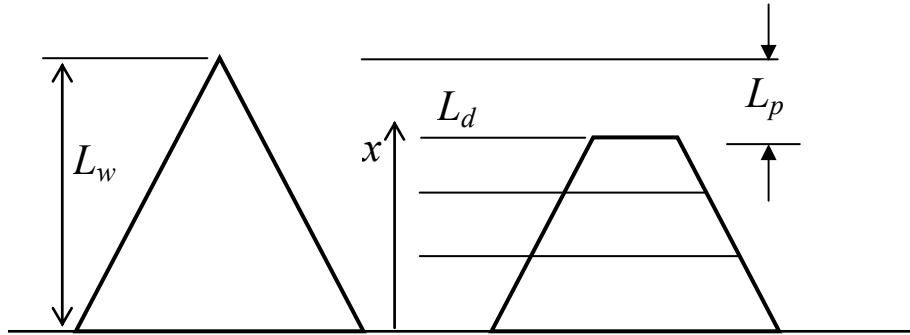


Figure 6. Mitigator wedge deformation zones.

The mitigator deformation can be expressed through the displacements of both its ends, which are equal to the displacements of the adjacent masses m_2 and m_3 .

$$\Delta L_0 = u_{OBR} - u_{MEM} \quad (7)$$

The plastic wave speed, c_{pl} , is equal to the time rate of change in length of the crushed portion as shown next.

$$c_{pl} = \frac{d(x + \Delta L_0)}{dt} = \frac{1}{\varepsilon_c} \cdot \frac{d(\Delta L_0)}{dt} = \frac{1}{\varepsilon_c} \cdot \frac{d(u_{OBR} - u_{MEM})}{dt} = \frac{(V_{OBR} - V_{MEM})}{\varepsilon_c} \quad (8)$$

Knowing the velocity of the OBR at time t_n , we can calculate this speed and revise the plastic wave front location:

$$(x_{front})_{n+1} = (x_{front})_n + (c_{pl})_n \Delta t \quad (9)$$

The stresses immediately below the plastic wave front (assuming a vertical mitigator with the wedge on top, figure 6) are equal to the yield stress. Thus, knowing the position of the wave front, one can easily determine the area at the plastic wave front (A_f) and the corresponding cross-sectional resultant contact force, F_{cont} as shown next.

$$F_{cont} = \sigma_y \cdot (A_f) \quad (10)$$

The front area, A_f , is determined from the plastic wave front displacement. Within the wedge portion of the mitigator, we assume that there are two regions: the plastic zone and the elastic zone. As illustrated in figure 6, L_w is the wedge initial height, and L_d is its current deformed height to be determined from loading. When the plastic zone length (L_p) is less than the wedge length (L_w), then the front area can be determined as follows:

$$A_f = A_o \frac{L_p}{L_w} \quad (11)$$

Otherwise,

$$A_f = A_o$$

in which A_o is the cross-sectional area of the cylindrical mitigator.

Equation 10 is assumed to represent the mitigator force, F , the contact force between the mitigator and OBR, and the mitigator and MEM in figure 2. Computation of mitigator force using equation 10 is believed to be valid to a sufficient degree of accuracy as long as the plastic wave front progresses forward ($c_{pl} > 0$). When the plastic wave motion no longer propagates, then the mitigator force decreases after the unloading of the elastic stiffness of the mitigator. This scheme can be easily programmed as a stand-alone routine, as shown in appendix A.

1.3.3 Strain Rate Effects

Any analysis model of the impact event would rely on the constitutive representation of the mitigator honeycomb. The associated relationship would usually be strain rate dependent, with the dependency being very important for the accuracy of representation. Significant stress enhancement under impact loading is reported for most of the cellular honeycomb materials by Zhao (4). Since in most cases it is impossible to develop a closed form model of the strain rate effect, some empirical approaches have been developed and successfully applied in this investigation. One such example is a power law relation used in (5), in which the stress is expressed as a function of

the quasi-static stress-strain relationship and of the current strain rate. Experimental data for different rates can be used to obtain the parameters of the power law relationship, thus expressing the stress enhancement as a function of variable strain rates. Since no such experimental data are available for the present study, the available quasi-static relations are used, and a stress enhancement coefficient of 1.5 times the static stress is assumed to model the crushing stress on the honeycomb material. In a previous finite element (FE) simulation of the air-gun environment (6), the authors have successfully demonstrated the effectiveness of such a constant stress enhancement factor of 1.5 in modeling the strain rate effect on the honeycomb material.

1.4 Results and Discussion

1.4.1 Validation of Present Model

To validate the present model and assess its performance, the predicted responses with the present model are compared with the available test and simulation results. Measured responses from the air gun launch simulation of the test item shown in figure 1b, as well as the results from a detailed FE model built to represent the system behavior of the air gun environment, are used for validation and verification of the present model.

To model the honeycomb material, the static stress-strain curve from figure 3 was used, scaled to 1.5 times the static relationship to incorporate the strain rate effect. This approach was identical to the one used in the FE analysis (6). The total mass of the OBR was distributed between the two masses m_1 and m_2 , with a ratio 1:1. To determine the k_1 (spring stiffness), the period of oscillation (T) of the OBR was estimated to be about 1.36×10^{-4} s, from the FE acceleration curve as filtered at 2500 Hz. The corresponding frequency was determined to be $1/T$, or 7353 Hz, and the angular frequency ω equals 46,200 rad/s. Then from equation 5 we have

$$k_1 = \frac{\omega^2(m_1 + m_2)}{4} = \frac{46200^2 \cdot 3.75}{4} = 2.0 \times 10^9 \text{ N/m}$$

The values of all parameters used in the present analysis are now provided:

m_1 – mass of OBR, back:	1.25 kg
m_2 – mass of OBR, front:	2.5 kg
m_3 – mass of MEM:	31.2 kg
k_1 – OBR spring stiffness:	2.0×10^9 N/m
v_0 – OBR initial velocity:	83.566 m/s
ΔT – End-time of analysis:	0.002 s
Δt – Time-step for analysis:	1.0×10^{-6} s
δt – Output time step:	4.0×10^{-6} s
ϵ_c – compacting strain:	0.64

σ_y – yield stress:	55.16 MPa
$\sigma_{crush} - 1.5 \cdot (\text{static yield}) = 1.5 \cdot 55.16 =$	82.74 MPa
E – elastic modulus:	4,060 MPa
ρ_0 – density of honeycomb:	650 kg/m ³
r – radius of mitigator:	0.05 m
L_w – length of mitigator wedge:	0.038 m
L_c – length of cylindrical section:	0.219 m

These values, converted for the convenience of comparing the results, were entered into the input file provided in appendix A. The analysis was performed with the FORTRAN (Formula Translator) program, and the corresponding results are presented and compared to the FE analysis and test results in figures 7 to 16. Figure 7 shows the unfiltered acceleration curves of the OBR top (attachment point of mass m_2 for present approach). Predicted accelerations filtered at 7000 Hz, 2500 Hz, and 1000 Hz are presented in figures 8, 9, and 10, respectively. Since the only frequency present in the current model is low, the results from the present approach have been filtered only in figure 10, which portrays the results of applying a 1000-Hz filter to all three curves. In figures 7 through 9, only the FE and test curves were filtered. As seen from the first two figures, the present approach matches the average of both the test and the FEA curves. Figure 9 shows that the present model gives excellent results for both the acceleration peak and the acceleration pulse duration. Figure 10, data filtered at 1000 Hz, indicates excellent agreement between the present and the FE approach. Figure 11 shows frequency domain plot comparison of the acceleration data. As seen in figure 11, the first fundamental frequency of the present model matches that of the test item. This comparison suggests that the modeling of OBR spring stiffness, k_1 , based on test item's first fundamental mode, reasonably captures the dynamics of the proposed mass-spring discrete system of the air gun launch environment.

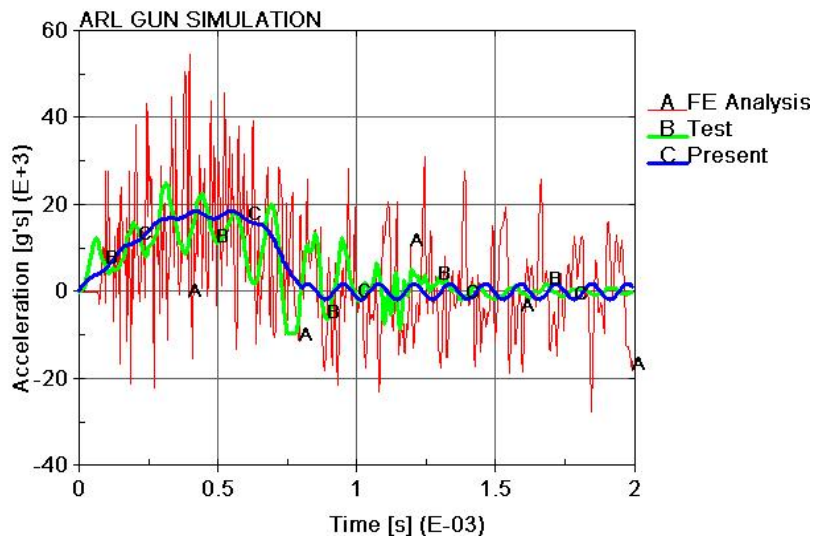


Figure 7. Top acceleration of the OBR unfiltered.

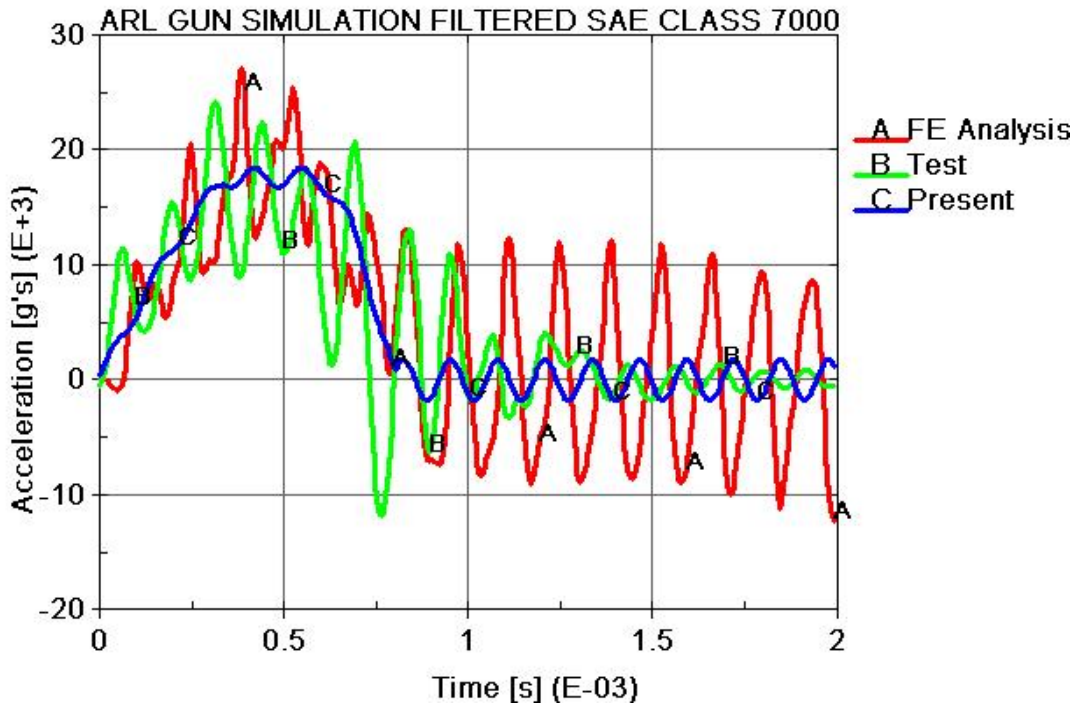


Figure 8. Top acceleration of the OBR filtered at 7000 Hz.

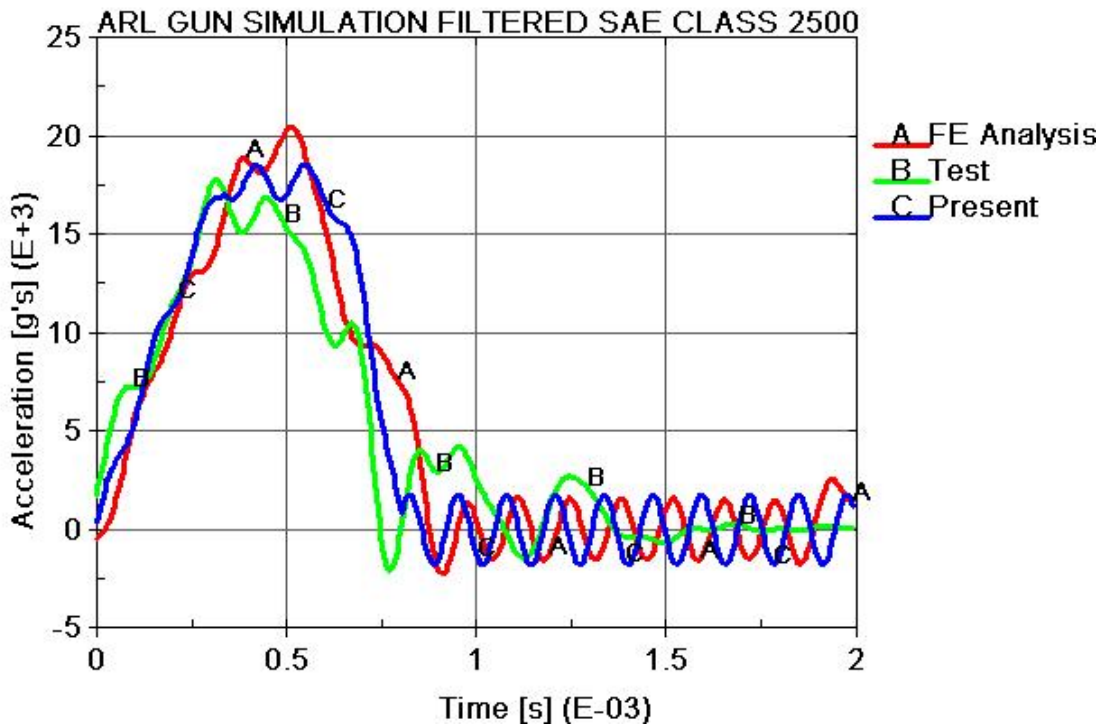


Figure 9. Top acceleration of the OBR filtered at 2500 Hz.

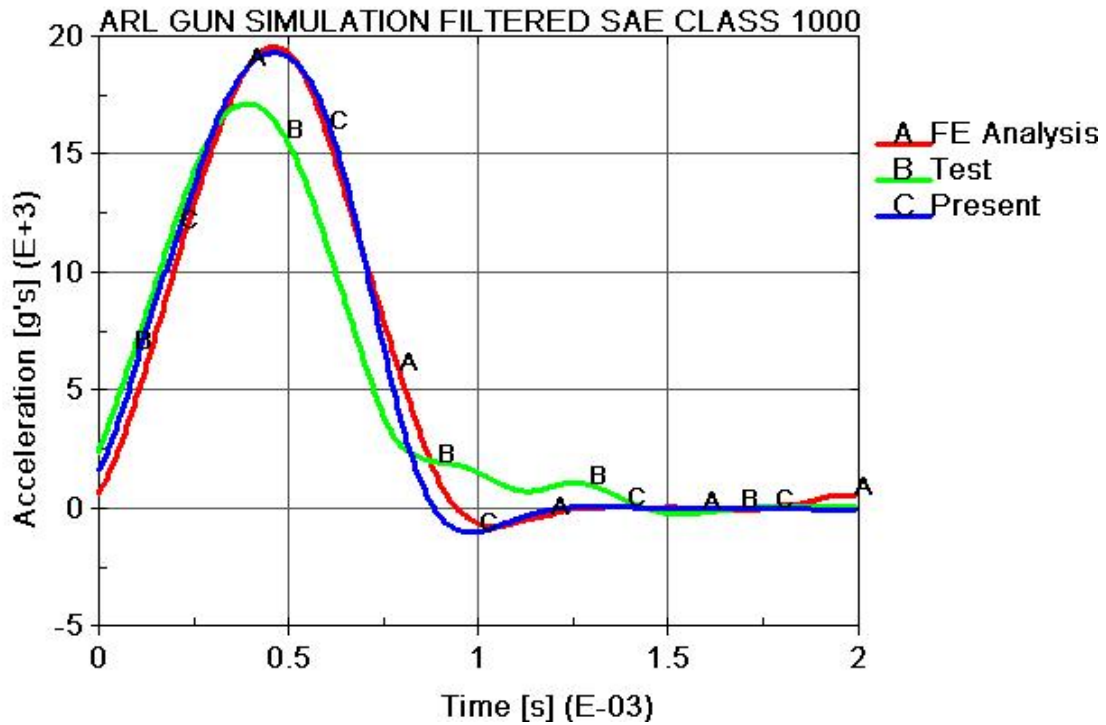


Figure 10. Top acceleration of the OBR filtered at 1000 Hz.

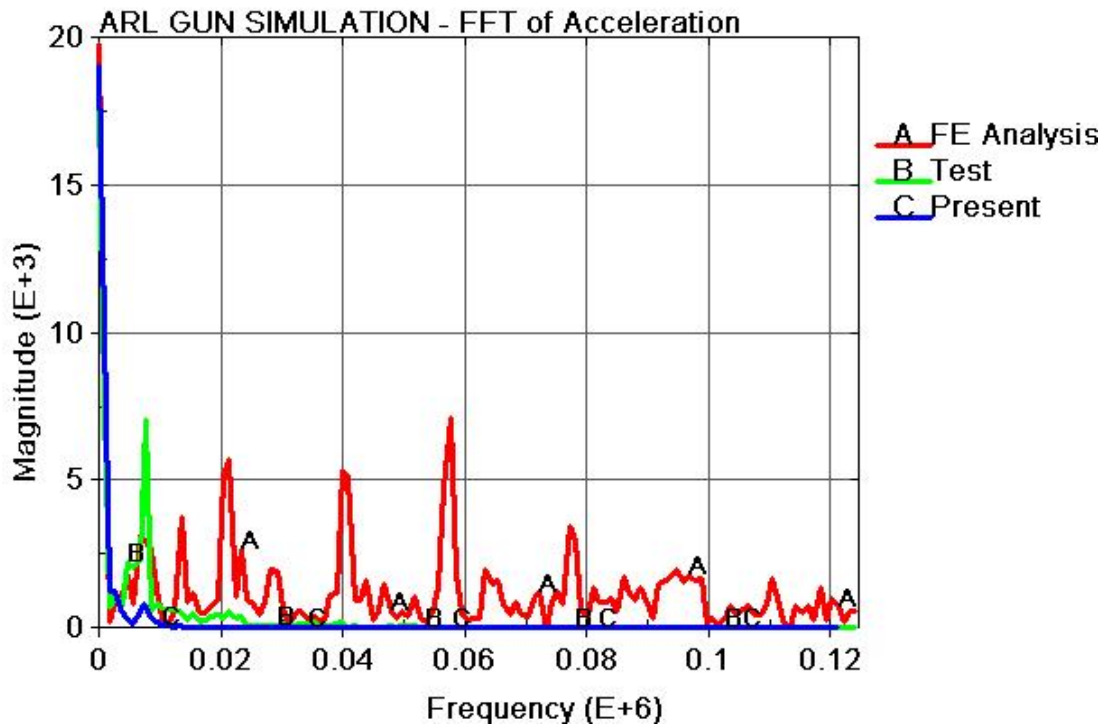


Figure 11. Fast Fourier transform (FFT) of the top acceleration of the OBR.

OBR velocities for the test, FE simulation, and present approach are compared in figure 12. As shown in the figure, a very good agreement is observed between the FE and present approach. Test velocity history is obtained from the integration of test acceleration data. A similar comparison of OBR displacement results for all three cases is presented in figure 13. Figure 13 shows that the present approach matches the maximum displacement from the test very closely. The discrepancies we observe to the right of the peak displacements (when the OBR starts to retract) can be attributed to friction in the “catch tube” and to other mechanisms not accounted for within the FE and the present analysis.

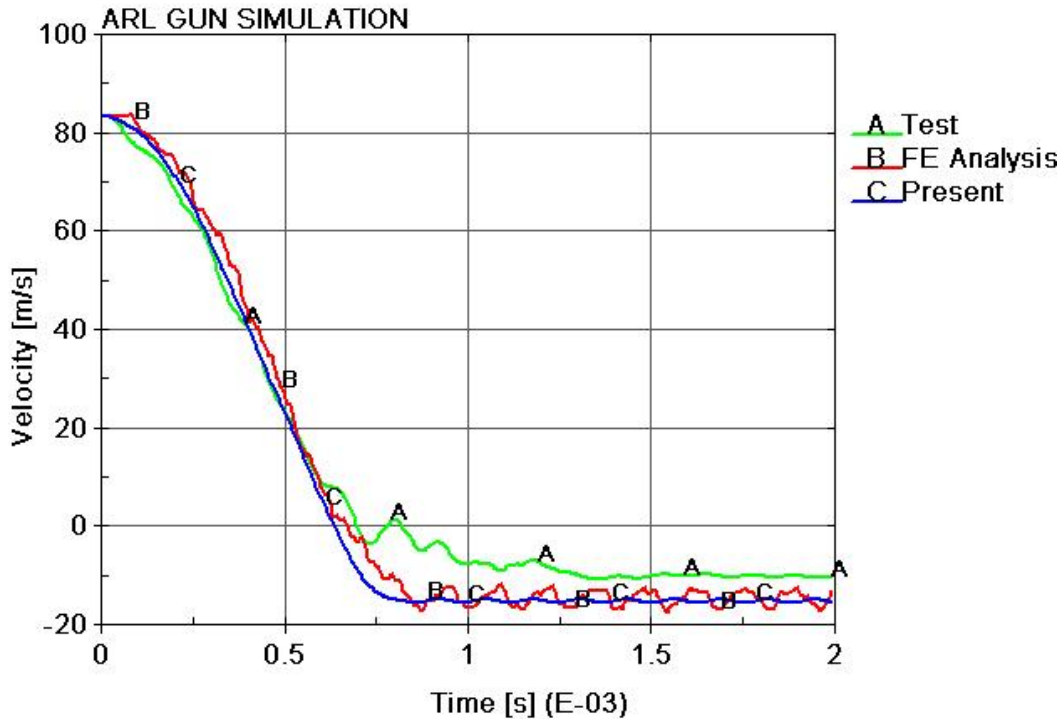


Figure 12. Top velocity of the OBR.

Figure 14 shows the contact forces between the mitigator and the OBR and between the mitigator and the MEM. In the FE analysis, these forces differ because of the elastic wave propagation speed, inertial effects in the mitigator, etc. These phenomena contribute insignificantly to the dynamics of the system, especially if the OBR is to be the primary object of interest; therefore, they were neglected within the present approach. This simplification makes the contact forces at the two interfaces equal, but as we see, they are very close to the average of both curves. Furthermore, when we compare impulses by integrating the force over time, we get a very good agreement among the impulses at both interfaces, as shown in figure 15.

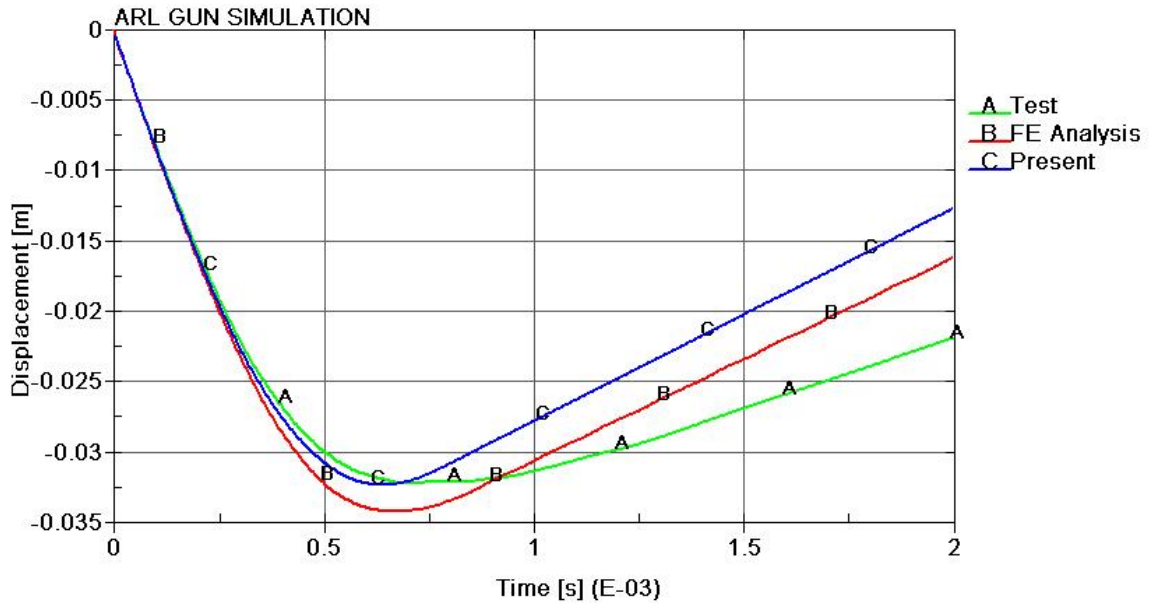


Figure 13. Top displacement of the OBR.

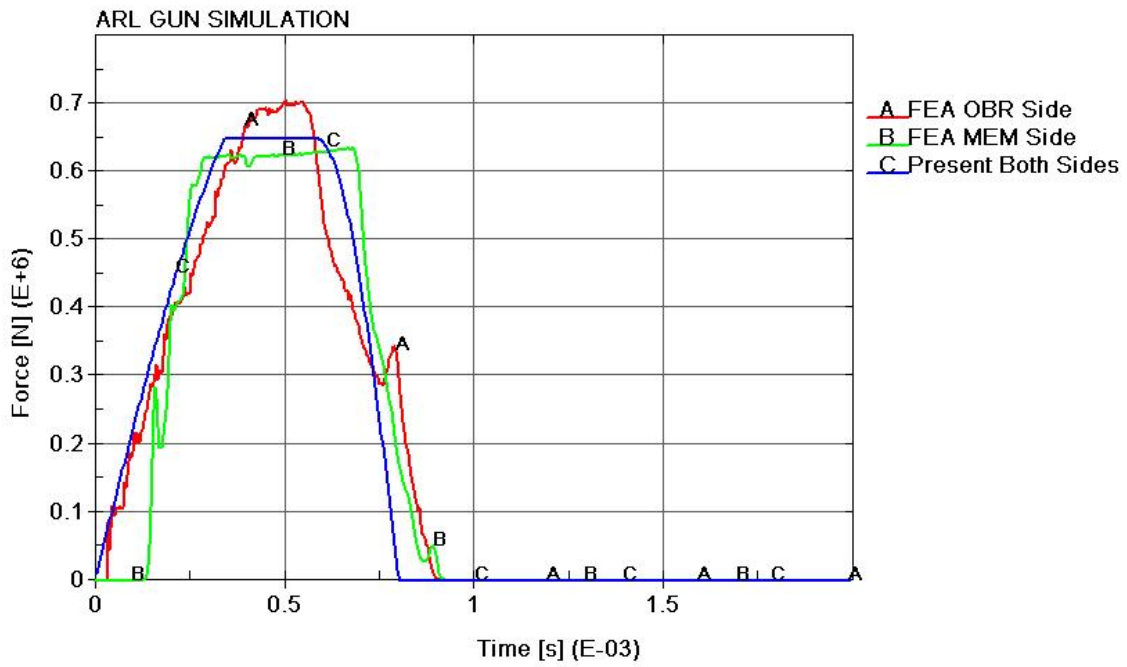


Figure 14. Mitigator contact forces.

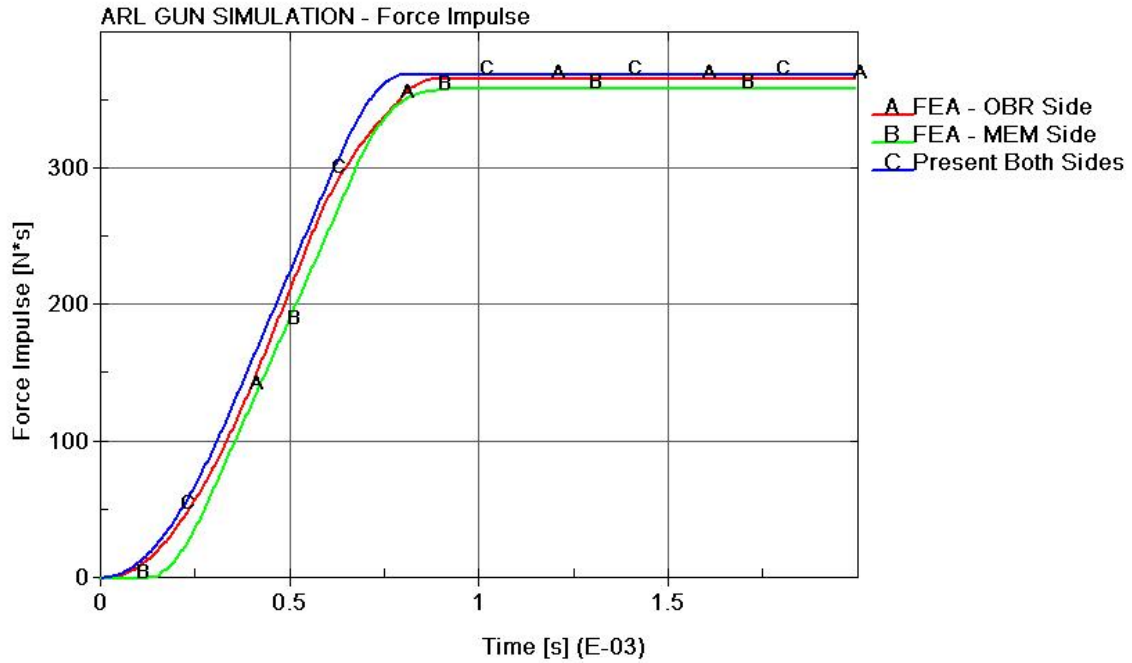


Figure 15. Mitigator contact force impulse.

The present approach provides data for the length of the compacted zone within the mitigator. The position of the crush front within the undeformed mitigator (“initial”) and the length of the crushed part (“compacted”) are shown in figure 16.

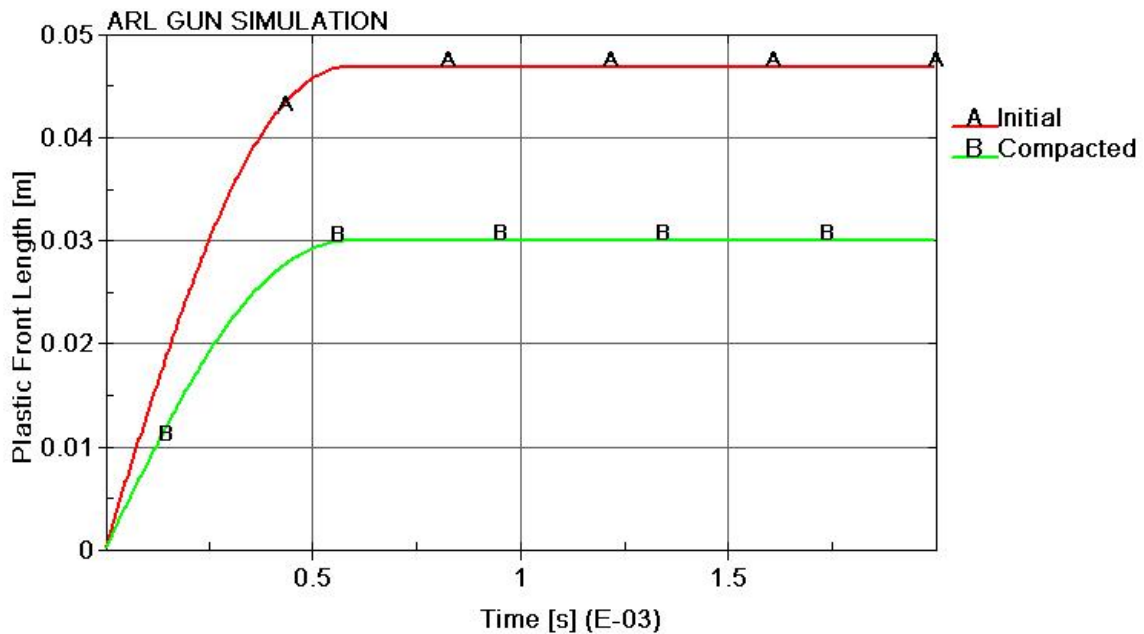


Figure 16. Length of mitigator plastic region.

1.5 Parameter Variation Sensitivity

In this section, we illustrate the model's response to varying the parameters of the system. As explained earlier, the representation of the OBR by two separate masses and a spring aims to capture one additional frequency of the OBR which is considered of interest. However, this representation requires the total physical mass of the OBR to be distributed between the two representative masses in the model: m_1 and m_2 . Furthermore, the connecting spring stiffness has to be determined. These processes introduce additional uncertainties into the model; this is especially true of the mass distribution process since it is not uniquely defined but depends on the user's judgment. In general, varying the $m_1:m_2$ mass ratio will only change the oscillation amplitude, not the oscillation frequency. Figure 17 shows the acceleration curves of masses m_1 and m_2 for two different distribution ratios. First, the total mass of the OBR (3.75 kg in this example) was distributed to 1.25 kg for m_1 and 2.5 kg for m_2 (ratio 1:2). The corresponding accelerations are shown with curves A and B in figure 17. Curves C and D show the accelerations of the masses for a ratio of 2:1 ($m_1 = 2.5$ kg and $m_2 = 1.25$ kg). The frequency of oscillation for all four curves is the same. Only the amplitude of oscillation is changed.

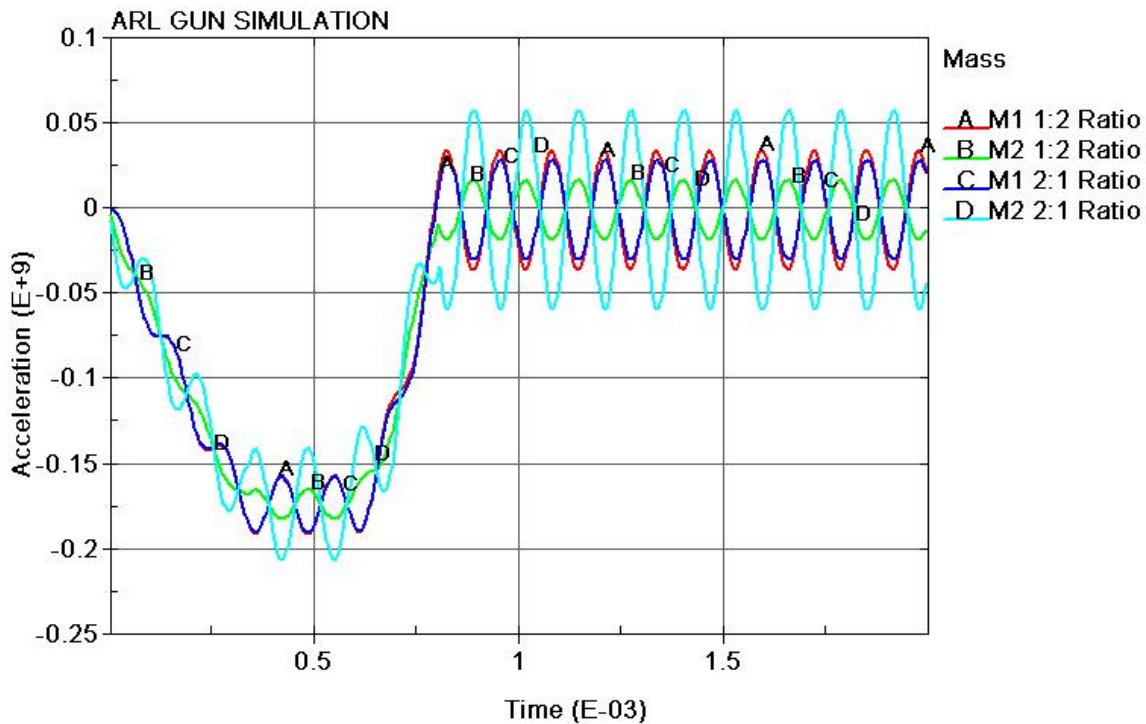


Figure 17. $m_1:m_2$ mass ratio sensitivity of model.

The stiffness of the spring connecting the two OBR masses, k_1 , is determined by equation 5 which requires the determination of the angular frequency of the OBR. Since this would normally be determined experimentally, some error might be introduced into the spring stiffness value. Therefore, it is interesting to see how small variations in the value of k_1 would affect the model output. Effects of the variation of k_1 values are illustrated in figure 18, which compares

the initial acceleration response to that obtained for k_1 values 10% smaller and larger than the initial stiffness determined by equation 5. As seen, the system behavior, especially in the area of interest (first millisecond), does not change significantly. Furthermore, when drastically changing the spring stiffness value, as shown in figure 19, we still get the correct shape and peak of the deceleration pulse.

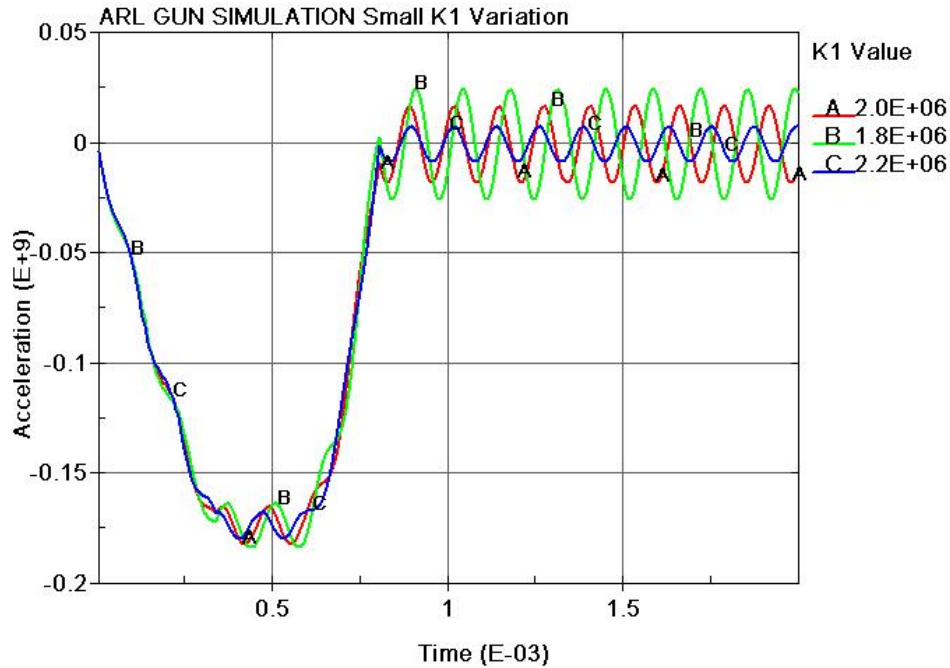


Figure 18. Model sensitivity to 10% variation of the value of k_1 .

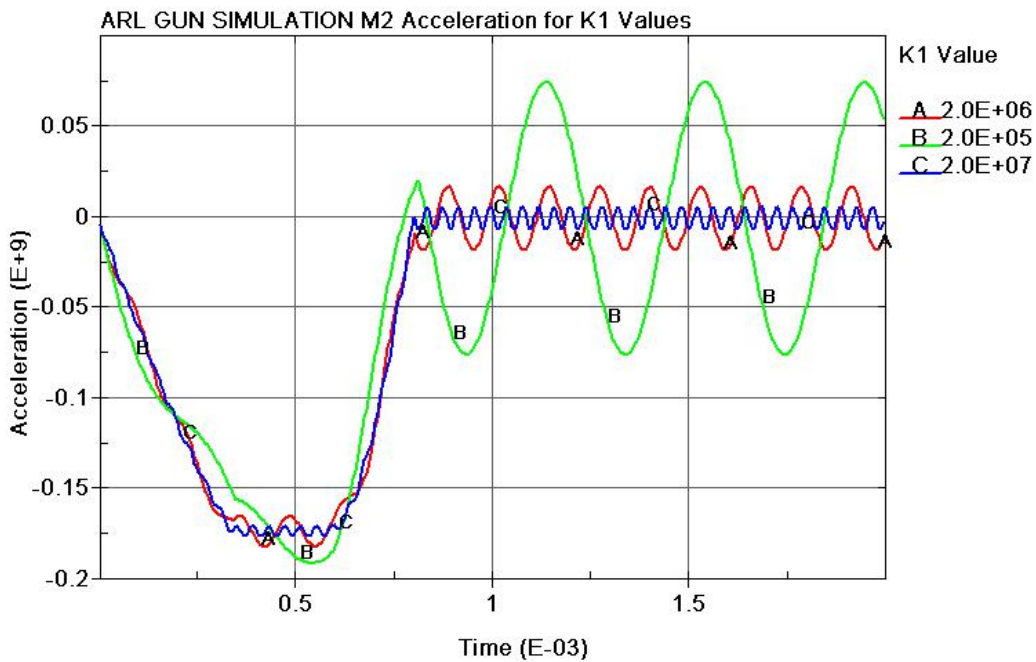


Figure 19. Model sensitivity to large variation of the value of k_1 .

The integration time step is a very important parameter of the central difference time-stepping scheme. In order to get an accurate solution, the time step needs to be smaller than a certain value called the critical time step. If this requirement is not satisfied, the solution quickly diverges. Therefore, determining the critical time step for a given solution is very important to ensure accuracy in the results. However, in most cases this is not an easy task, and for complex systems, only threshold limits of the critical time step are determined. In the present model, there is no need to determine the critical time step explicitly. Since the solution does not take a significant amount of run time, we can easily re-run it with a smaller time step and compare the two solutions to assess the accuracy of the results. As illustrated in figure 20, the initial solution using a time step $\Delta t = 1.0 \times 10^{-6}$ s is identical to the solution generated with a 10-times-smaller time step, $\Delta t = 1.0 \times 10^{-7}$ s. Even with a much coarser time resolution of $\Delta t = 2.0 \times 10^{-5}$ s, we get a reasonably accurate solution. This shows that the chosen value of the time step is well below the critical and illustrates the good overall stability and robustness of the solution scheme.

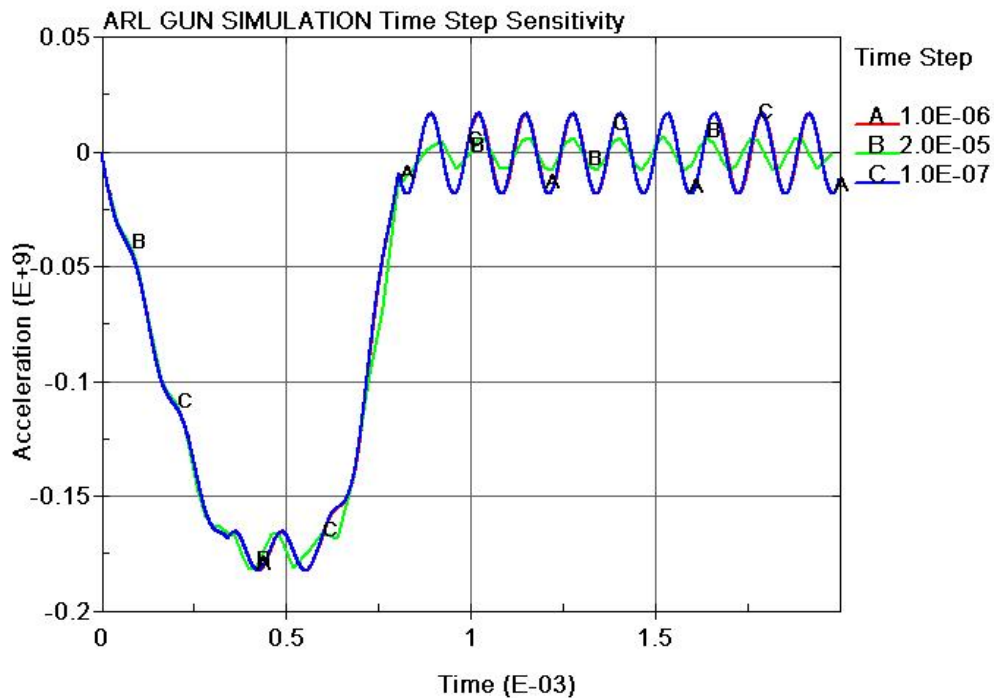


Figure 20. Model sensitivity to variation of the solution time step.

Finally, to illustrate how some of the geometric parameters of the system affect the solution response, the radius of the mitigator honeycomb cylinder was varied. The corresponding OBR acceleration responses are shown in figure 21. As would be expected, a smaller radius produced a lower acceleration peak and a wider pulse, whereas a larger radius produced a higher acceleration peak and a narrower pulse.

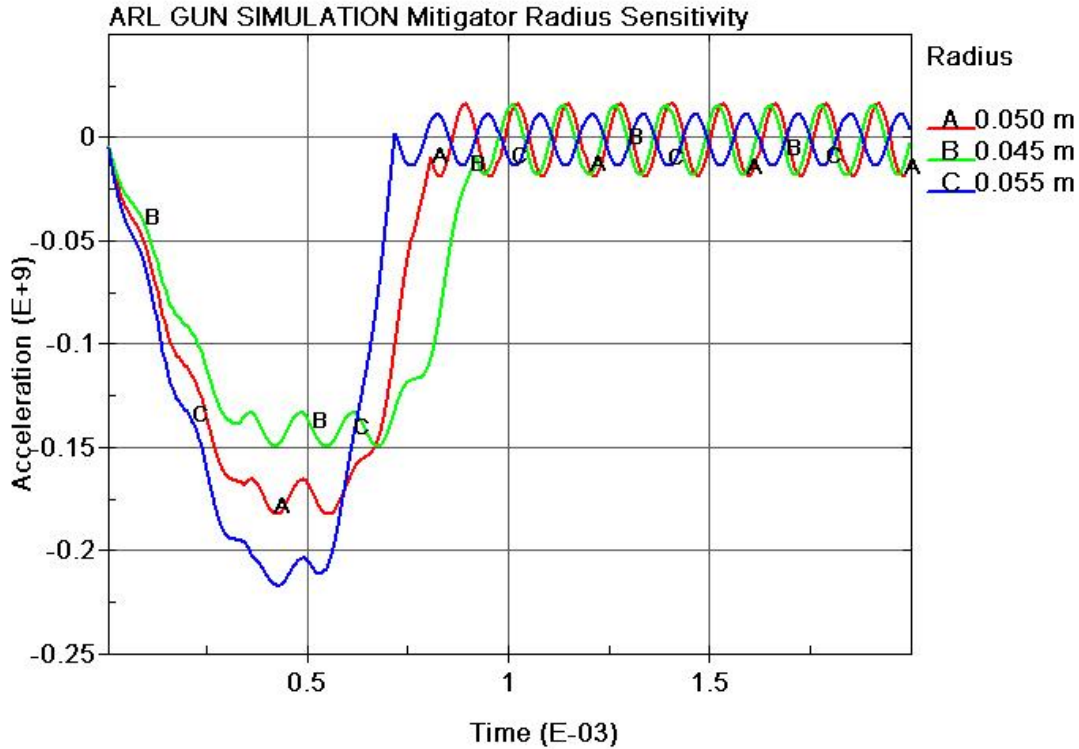


Figure 21. Model sensitivity to 10% variation of the value of mitigator radius.

1.6 Conclusion

The objective of this effort was to develop an overall analytical model to predict the transient response of a generic artillery component subjected to launch simulation. The simulation is achieved by impact mitigation techniques in which the component is propelled to a target inside a carrier equipped to measure component response during the simulation. A 2-degree-of-freedom model is developed to simulate the air gun launch environment in which a test object mounted on a projectile is fired through the air gun and decelerated by the crushing of an aluminum honeycomb mitigator, which in turn impacts the MEM before being stopped at the retrieving end. The presented model achieved a good prediction of the period and peak acceleration of the OBR.

Sensitivity of parametric study indicates that the distribution of masses in the spring-mass model of the test item does change the oscillation amplitude without affecting the system's frequency of vibration. A slight variation of spring stiffness ($\pm 10\%$) does not change the shape and neither does it affect the peak of the deceleration pulse of the test item. The sensitivity study of initial time step illustrates the good overall stability and robustness of the proposed solution scheme.

2. Part II: Air Gun Finite Element Simulation

2.1 Review of Previous Work

Several LS-DYNA models were developed to simulate an air gun launch environment. In this test, a test object is mounted on a projectile and fired through the air gun. The object is decelerated by the crushing of an aluminum honeycomb mitigator MEM complex before being stopped at the retrieving end (6).

The objective of the effort was to develop an overall simulation model to predict the three-dimensional transient response of a generic artillery component subjected to launch simulation in the U.S. Army Research Laboratory's air gun facility at Adelphi, Maryland. The simulation is achieved by impact mitigation techniques whereby the component is propelled to a target inside a 4-inch carrier equipped to measure component response during the simulation. These models include all elements of the simulation apparatus that contribute to the total response of the component under test.

Two formulations are employed in the simulations: Lagrangian and arbitrary Lagrangian/Eulerian (ALE). The aluminum honeycomb mitigator undergoes a significant amount of deformation, which could render a Lagrangian simulation severely unstable. For this reason, an ALE simulation is also considered. The Eulerian method is more suitable for problems involved in severe mesh distortion. The Lagrangian method, on the other hand, is limited in how much an element can deform. The Lagrangian method is easy to set up and visualize since the material point moves with the mesh. However, the Eulerian method is more difficult to set up and the mesh is stationary so that material points are advected from one element to the next.

The aluminum honeycomb mitigator is modeled with *MAT_MDIFIED_HONEYCOMB in the LS-DYNA simulation code. This is material model number 126 in the code. This material model is available for the Lagrangian method only and it is not yet implemented in the Eulerian solver of the LS-DYNA. Therefore, an alternate material model is considered that can simulate the behavior of aluminum honeycomb and is available in the LS-DYNA Eulerian solver. The material model considered for this case is *MAT_CRUSHABLE_FOAM which is material model number 63 in LS-DYNA. This material model can simulate an isotropic crushable material. The *MAT_MDIFIED_HONEYCOMB can simulate an orthotropic crushable material. Most of the aluminum honeycomb material in the air gun simulation is crushed axially. Therefore, the *MAT_CRUSHABLE_FOAM model is considered to be appropriate for this model. Several LS-DYNA models are developed to simulate the air gun launch environment with Lagrangian and ALE computational methods. The Lagrangian method is simpler to set up, simpler to post process, and require less computational time. However, it requires significant expertise in the explicit FE codes to make the simulation numerically stable. This is because of the significant

large deformation of the mitigator. On the other hand, the ALE method is more difficult to set up, more difficult to post process, and requires much more CPU (central processing unit) time. However, the ALE simulation is more suitable for very large deformation-like flow problems. Both computational methods lead to the same prediction for the acceleration of the OBR. An accurate prediction of the period and peak acceleration of the OBR is achieved with the presented models and the methods employed.

2.2 Finite Element Model Sensitivity Study

It is very important that the FE simulation captures the contributions of high frequency oscillations to the net acceleration of the model. This will allow failure mode simulation of the embedded MEMS (micro-electrical-mechanical systems). Improving the correlation between test and FE results allows the FE simulation to become a tool for detecting/predicting failure modes of physical components subject to an air gun test. For this purpose, the developed FE model is further examined to fully understand the differences between the model and the experimental data and to acquire more confidence in the predictability of the simulation. Several model sensitivity issues are considered in detail as follows:

- double versus single precision code,
- time step size effect,
- different output intervals,
- different damping options in LS-DYNA (all options are investigated),
- representation of the OBR's glass beads with solid elements, and
- intermittent eigenvalue analysis.

Each one of these items is studied in detail, and the corresponding results are presented.

2.2.1 Double Versus Single Precision Code

The default LS-DYNA code is a single precision code. When the integration time step is small enough to satisfy the Courant stability condition, many integration cycles are possible. Since the LS-DYNA code is an explicit code based on second order central difference equations, numerical error propagation is possible. The same model was run with single and double precision code. The results are presented in figure 22. Fast Fourier transforms (FFTs) of the results are presented in figure 23. One can observe that both codes give the same results.

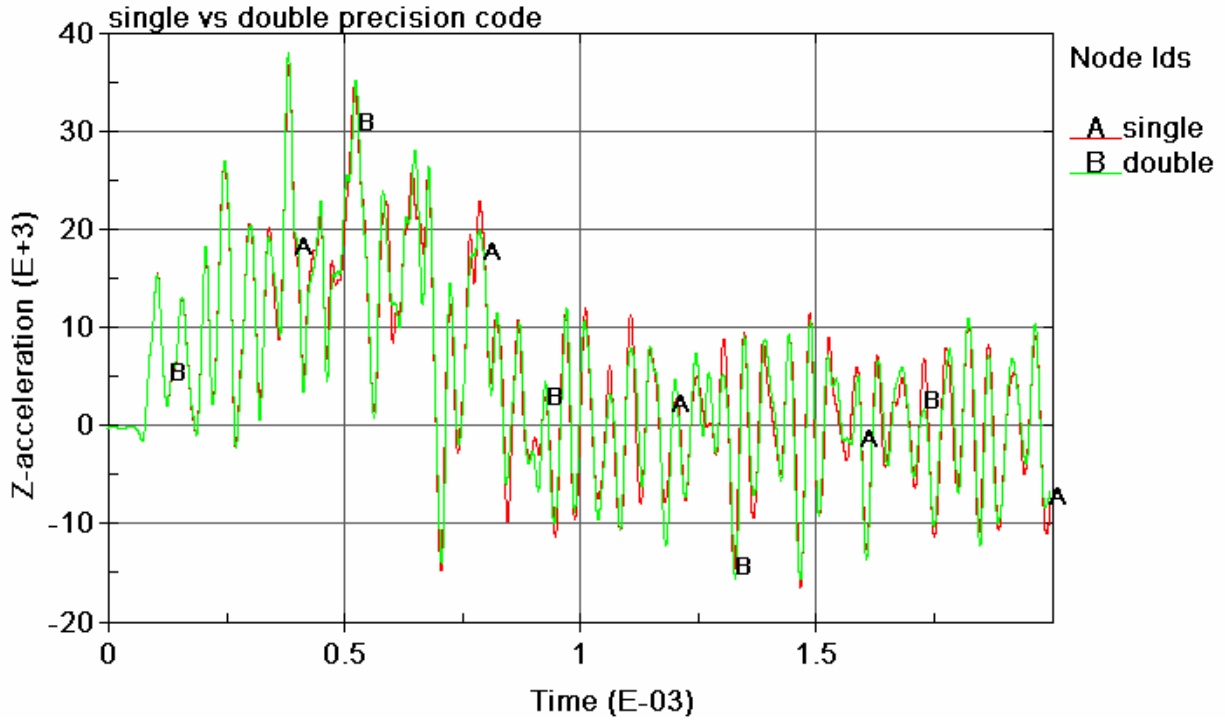


Figure 22. Acceleration data for the same FE model with two different precisions.

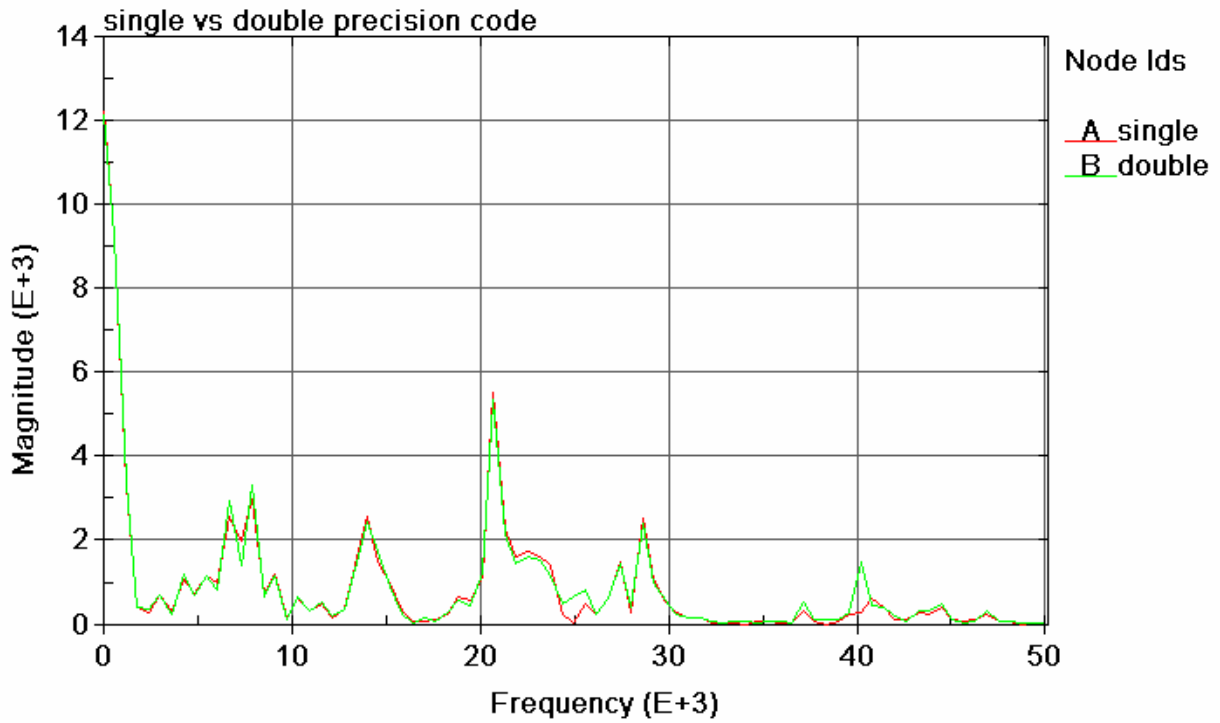


Figure 23. FFT of the acceleration data.

2.2.2 Time Step Size Effect

Integration time step size variation is used to measure the stability of a model. Time step variation is also used to detect any anti-aliasing in the collection of the data from the explicit time integration simulation. The default integration time step is normally taken to be 90% of the stability limit to avoid any filtering error such as beating in the data. This report considers two additional integration time steps. One is taken to be 80% of the critical time step and the other is taken to be 40% of the critical time step. The results of all three time steps are depicted in figure 24. FFTs of the data are depicted in figure 25. One can observe that all the important frequencies are the same in all the considered integration time steps. Therefore, the default integration time step is appropriate for this problem.

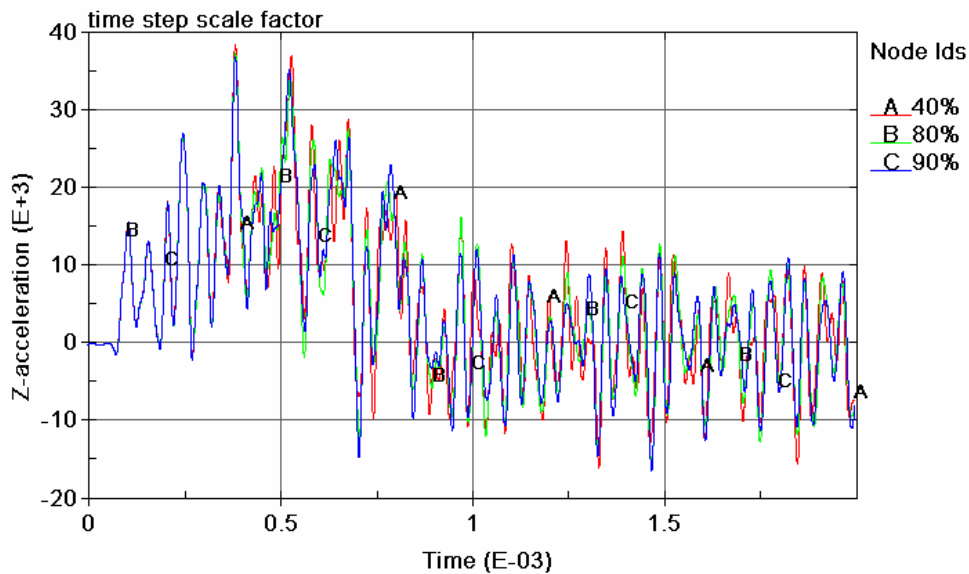


Figure 24. Acceleration data for different integration time steps.

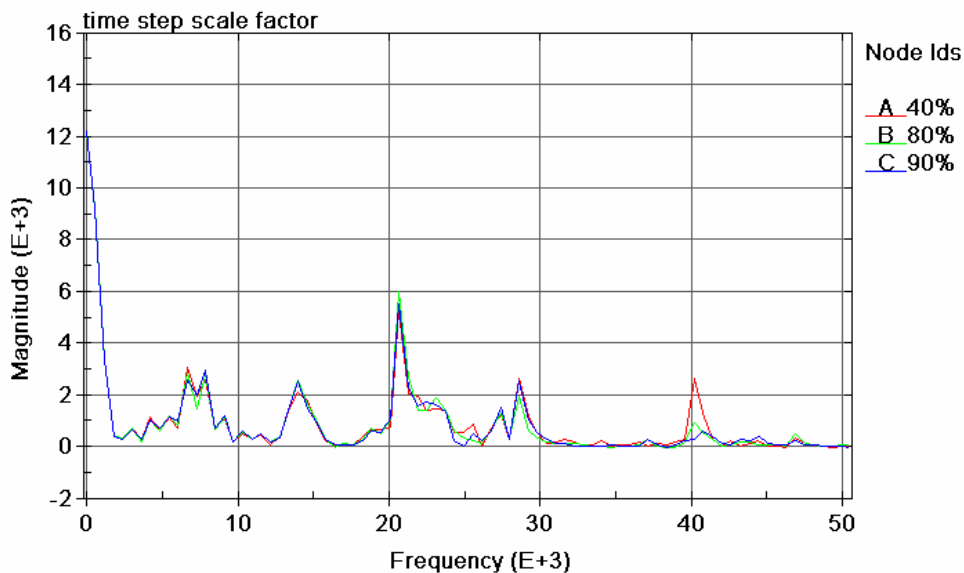


Figure 25. FFT of the acceleration data for different integration time steps.

2.2.3 Different Output Intervals

The data collection from the FE simulation should be the same as the test setup; therefore, the two data can be compared meaningfully. The sampling rate in the test is 4×10^{-6} seconds, which corresponds to 500 data sampling points in the 2-millisecond simulation. To investigate if any data are missing from the simulation or if any abnormality exists in the numerical calculations, data sampling rates of 10 and 20 times the test sampling rate are considered (5,000 and 10,000 points, respectively). In addition, data are collected at every integration time step. Figure 26 depicts the acceleration data for the entire sampling rate considered. FFTs of the data are depicted in figure 27. All major contributing and significant frequencies are present in the lower rate, which is also the sampling rate of the experimental data.

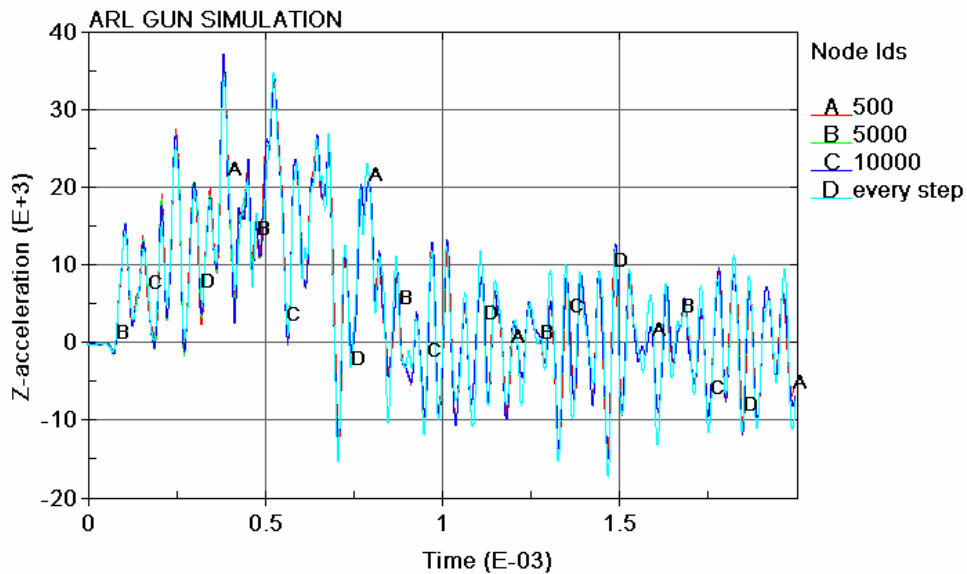


Figure 26. Acceleration data sampled at different frequencies.

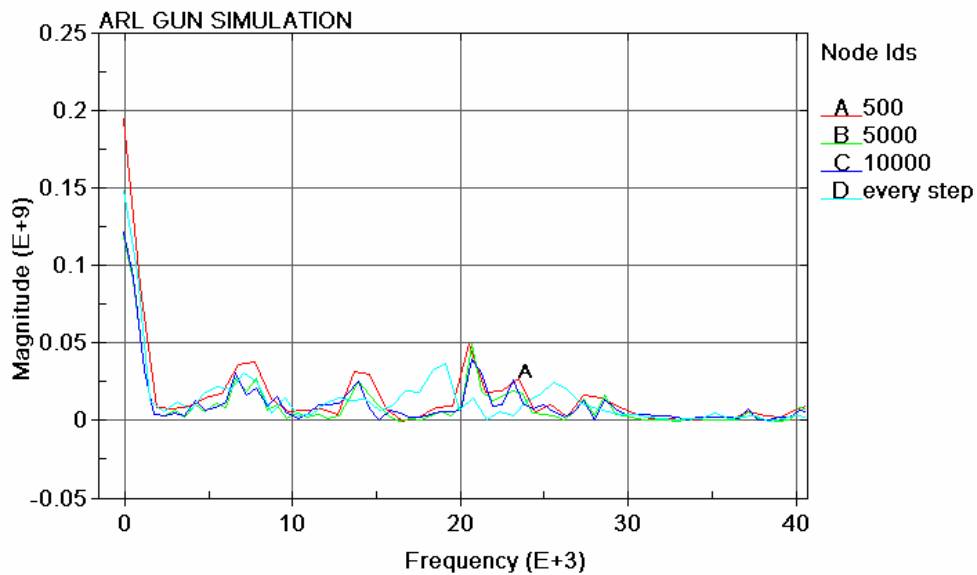


Figure 27. FFT of the acceleration data sampled at different frequencies.

2.2.4 All Damping Options in LS-DYNA Investigated

There are three options for damping in the LS-DYNA code: global, mass, and stiffness proportional damping. Global damping is similar in formulation as the mass proportional damping, and therefore, results for this case are not presented. Different damping constants are considered for each damping option. For the mass proportional damping, constants of magnitudes 100, 500, 1000, and 1500 are considered. Results for these cases are depicted in figure 28. FFTs of the acceleration data are depicted in figure 29. One can observe that frequencies are damped significantly, especially the lower frequencies of the system. Figure 30 depicts the test data and the damped acceleration data from the simulation.

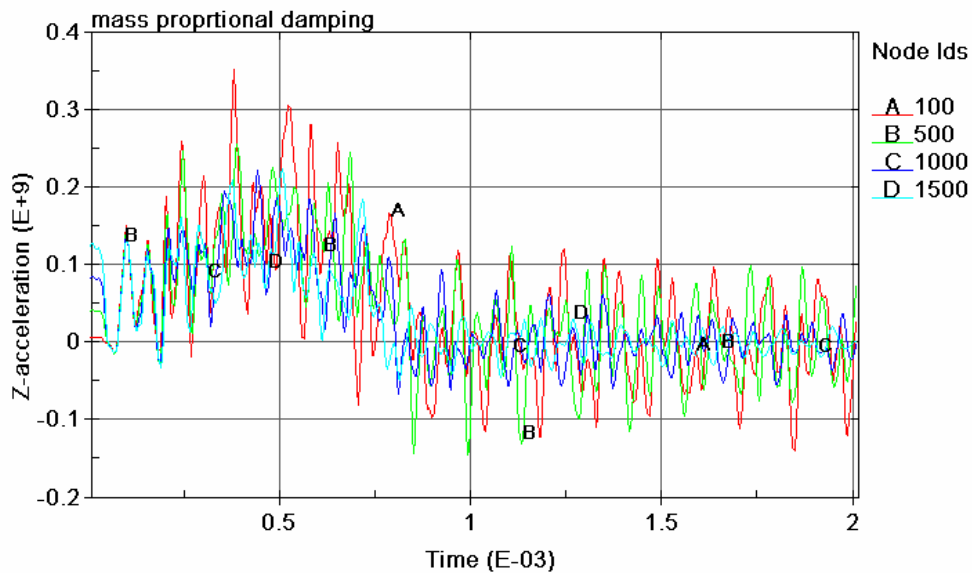


Figure 28. Acceleration data for simulation with mass proportional damping.

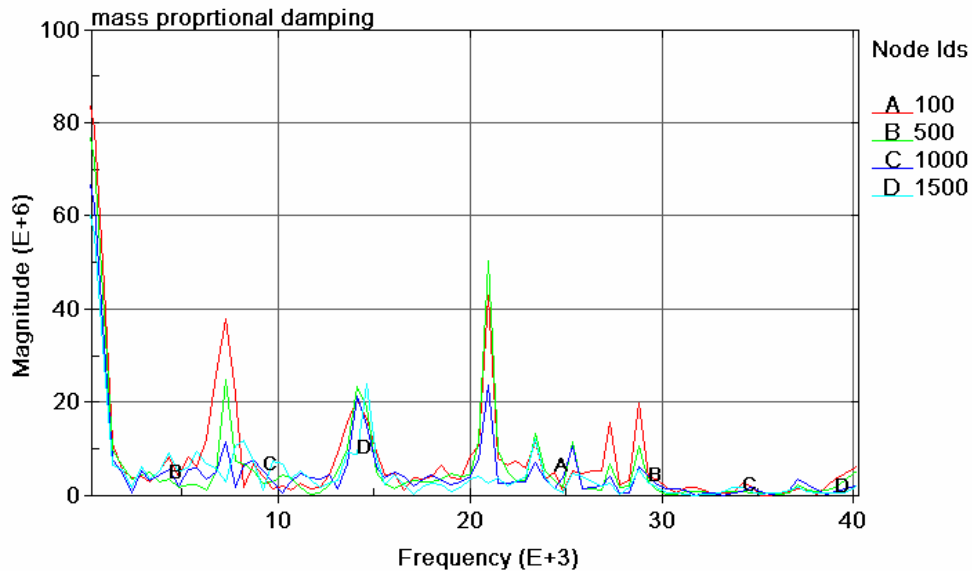


Figure 29. FFT of the acceleration data for simulation with mass proportional damping.

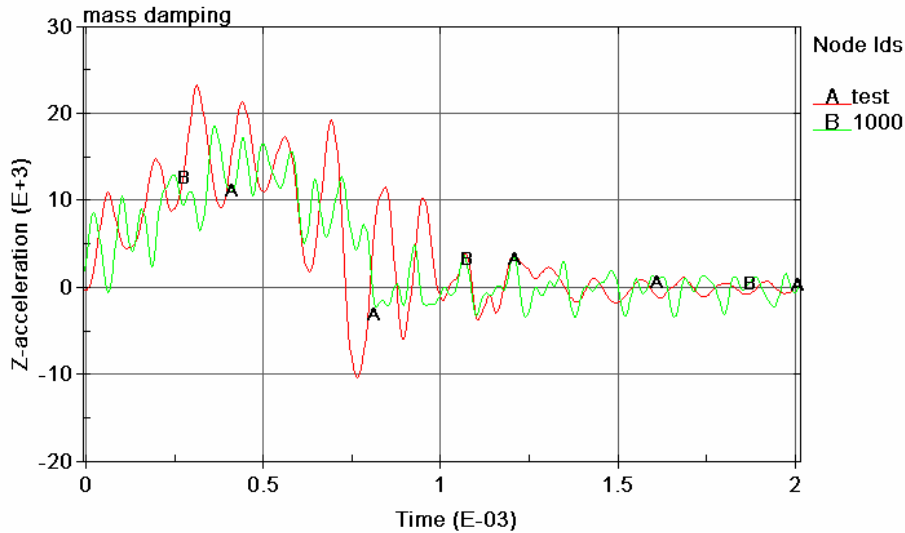


Figure 30. Acceleration data for simulation and test with mass proportional damping.

Stiffness proportional damping is considered in the simulation as 1%, 10%, 25%, 25%, and 35% of the critical damping. The acceleration data are depicted in figure 31. FFTs of the data are presented in figure 32. One can observe that the low frequencies are not damped, while the higher frequencies are damped. Figure 33 depicts accelerations from the test data, the simulation with no damping, and the simulation with 10% of the critical damping. Figure 34 depicts the FFT of these accelerations. One can observe, again, that higher order frequencies are affected more significantly than lower order frequencies. In general, mass proportional damping should be used for low frequency content and pure deformation with no rigid body motion since it damps the rigid body motion. Stiffness proportional damping is orthogonal to rigid body motion and would not affect this type of motion. Stiffness proportional damping is good for high frequency content and should be used in such problems where attenuation of high frequency vibration is desired.

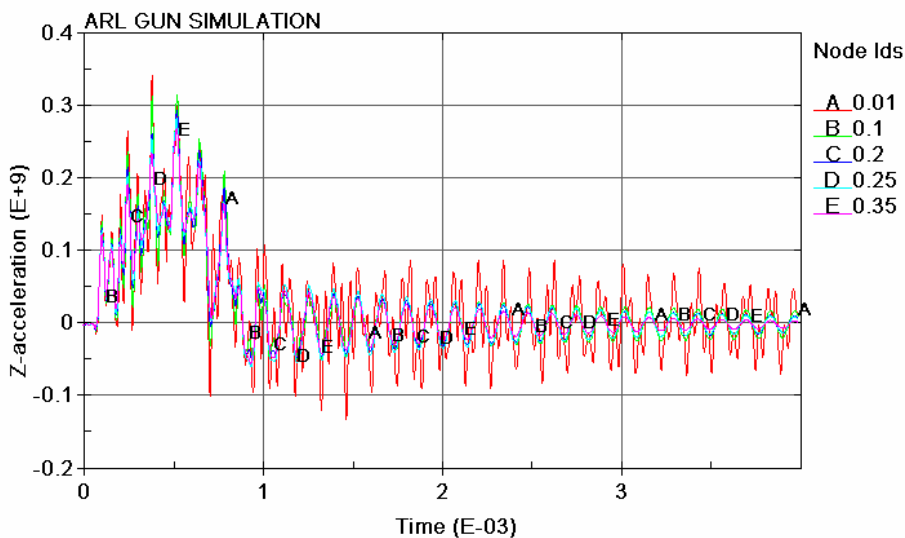


Figure 31. Acceleration data for simulation with stiffness proportional damping.

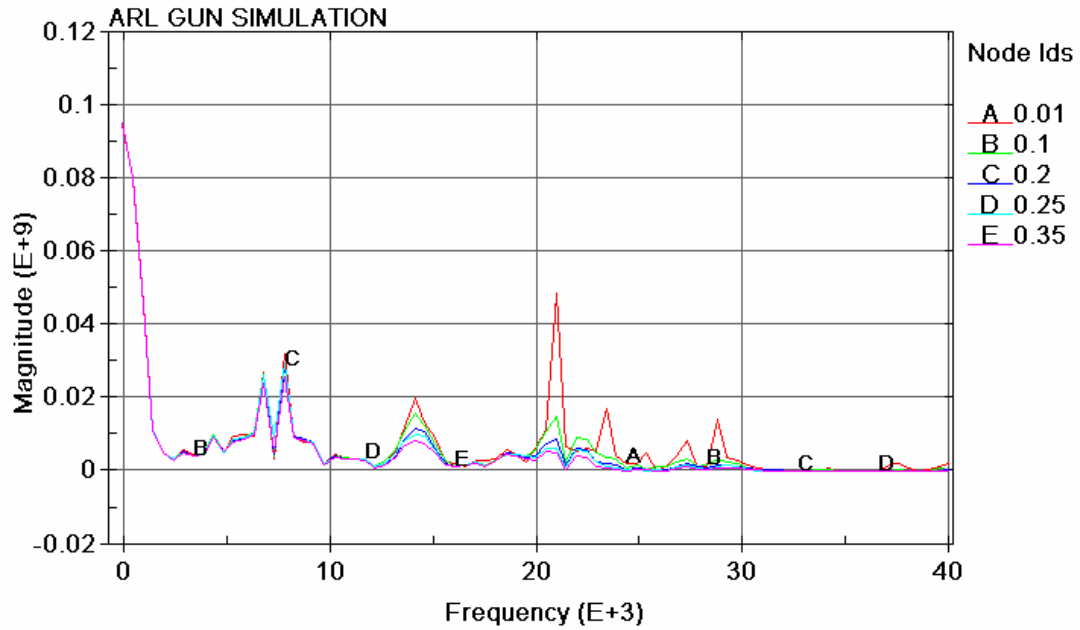


Figure 32. FFT of the acceleration data for simulation with stiffness proportional damping.

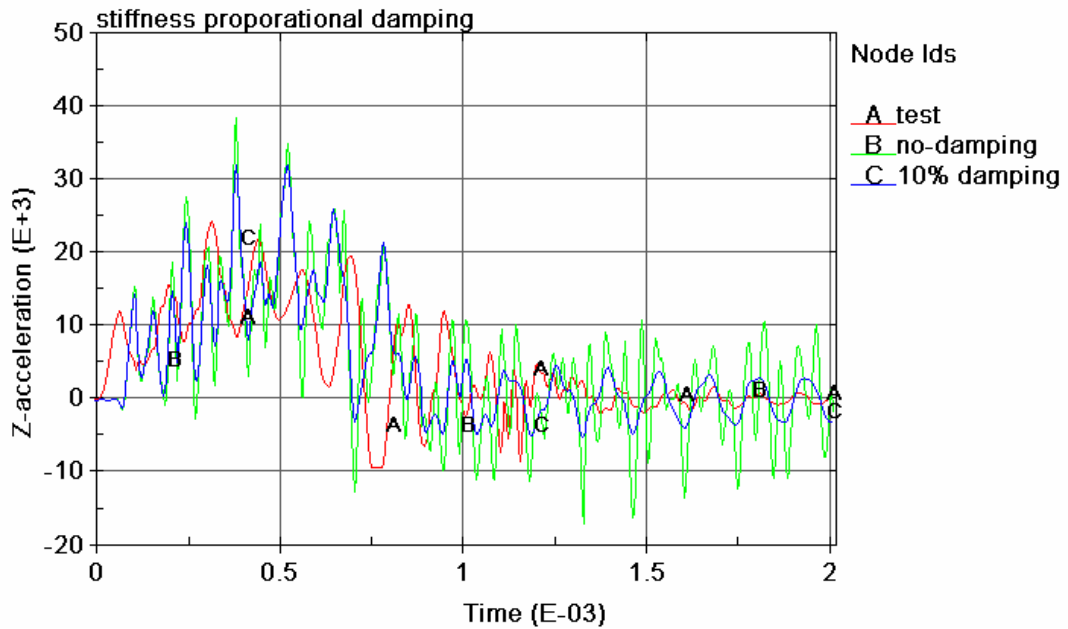


Figure 33. Acceleration data for simulation and test with stiffness proportional damping.

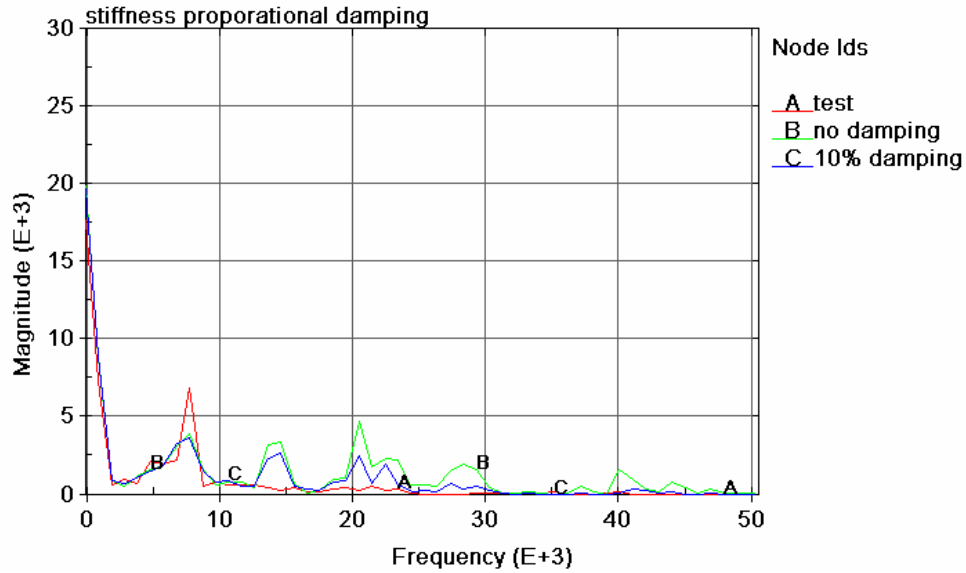


Figure 34. FFT of the acceleration data for simulation and test with stiffness proportional damping.

2.2.5 The OBR Filled With Solid Elements to Represent Beads

The OBR is filled with beads in the experiment. However, the OBR is hollow in the simulation. These beads exist in the OBR to protect the accelerometer during tests. There is no material model in any FE code to represent the behavior of these beads. In this report, a model of the OBR is considered that is filled with solid elements. Different material models such as soil, foam, viscoelastic, and crushable foam are considered for the beads in order to simulate the beads' damping high frequency oscillations. Results of the simulation are depicted in figure 35. One can observe that high frequency oscillations are more significant because of waves traveling back and forth in the solid element.

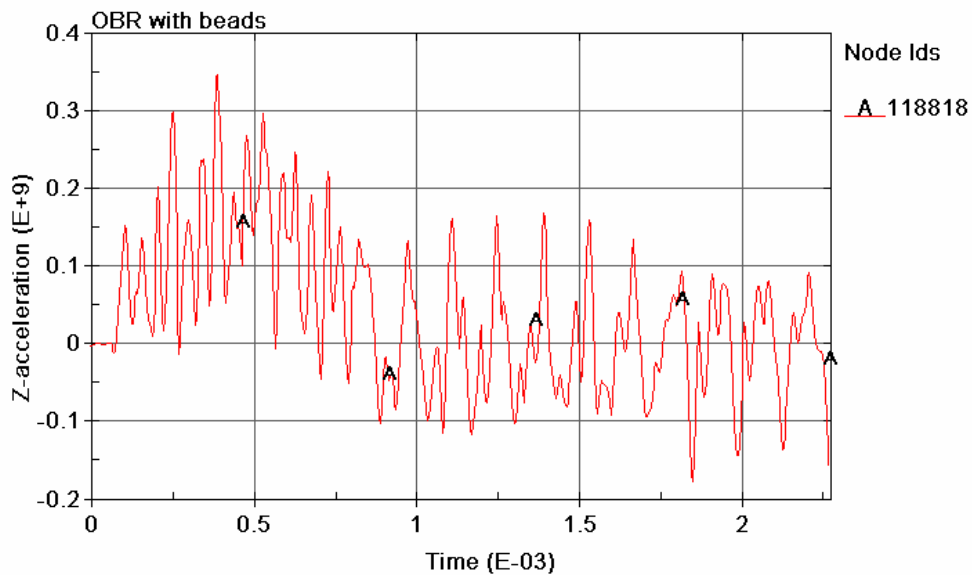


Figure 35. Acceleration data for simulation with filled OBR.

2.2.6 Intermittent Eigenvalues Analysis

To understand the frequency content in this simulation, an intermittent eigenvalue analysis is conducted. The LS-DYNA code allows for the extraction of frequency contents during an impact simulation. This is performed to relate the frequency content to the event and deformation mode in the OBR. The FFT of the unfiltered acceleration of the OBR is depicted in figure 36. One can see several important peaks in the data. The largest peak corresponds to the first fundamental mode. The next peak is at about 7400 Hz. The next ones are at about 8000, 14600, 21000, 23800, 27700, and 29500 Hz. The intermittent eigenvalue analysis revealed the sources of these frequencies. One hundred modes were extracted from the analysis. Only the modes corresponding to the peaks in the data are presented here. Figure 37 depicts the undeformed (line mesh) and the deformed mode (solid shaded mesh) corresponding to the peaks in the frequency spectrum graph (figure 36). It is clear that these peaks correspond to the axial mode of the OBR. High frequency content was not observed in the experimental data. However, high frequency content is observed in the simulation data. Since the beads are not present in the simulation and the high frequencies are attributable to the axial deformation modes of the OBR, one can conclude that these high frequencies in the simulation results are not realistic. This conclusion is based on the assumption that high frequency oscillations in the axial direction of the OBR are absorbed by the glass beads surrounding the accelerometer.

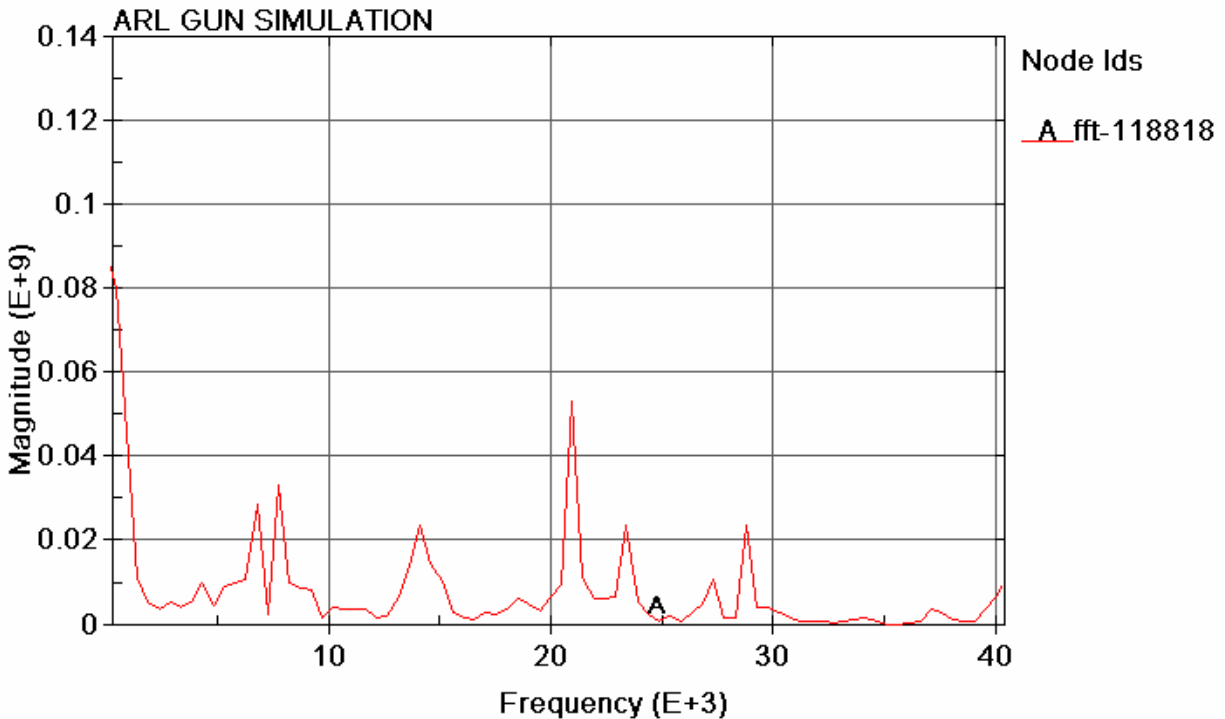
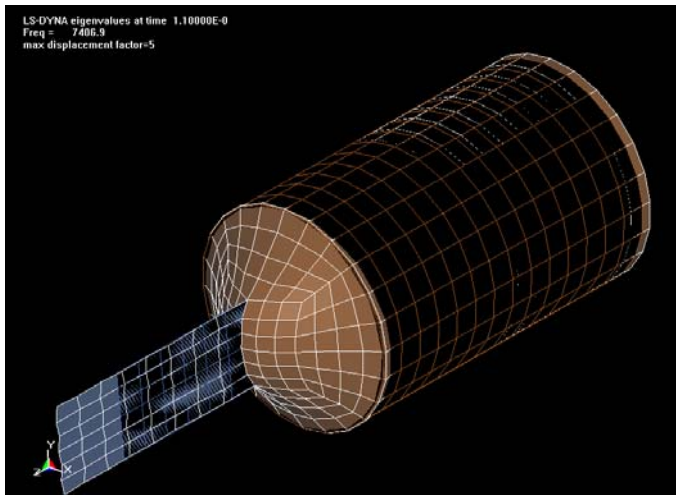
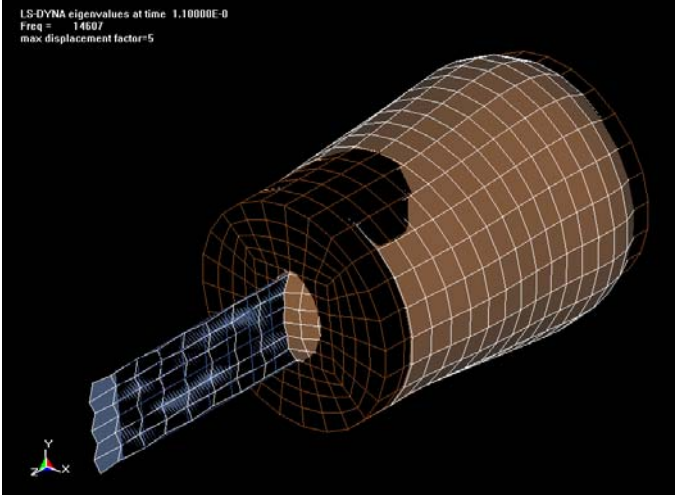


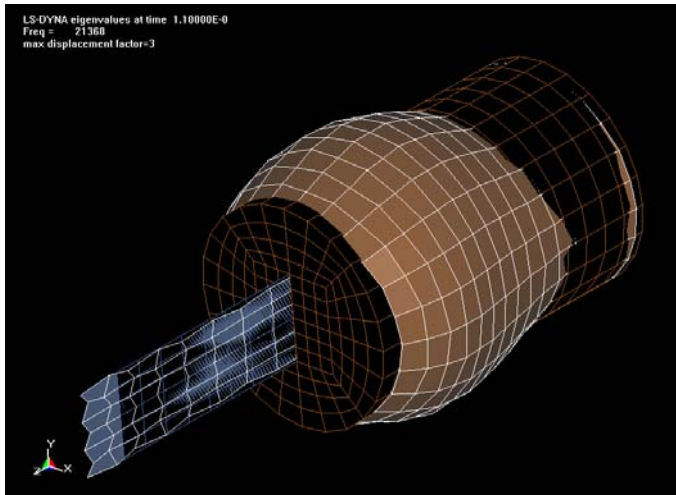
Figure 36. FFT of the acceleration data for simulation



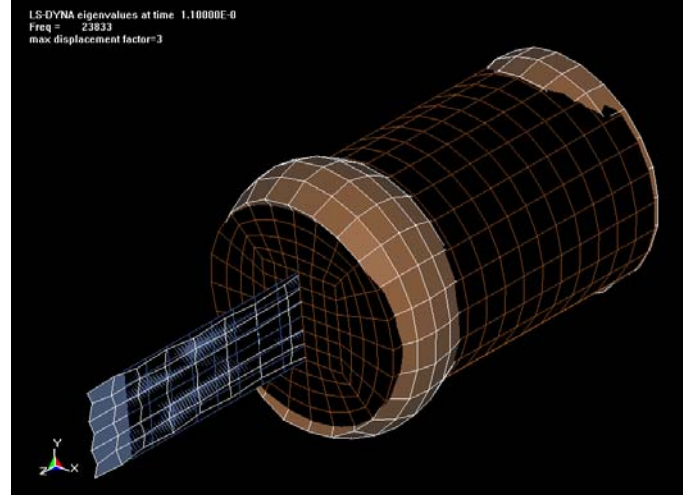
a.



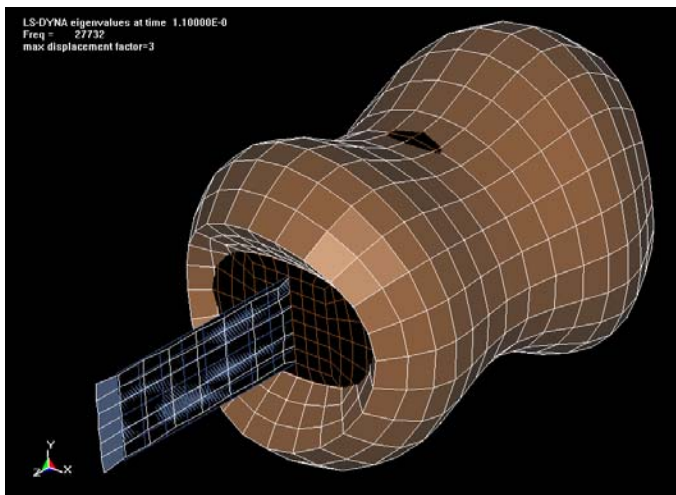
b.



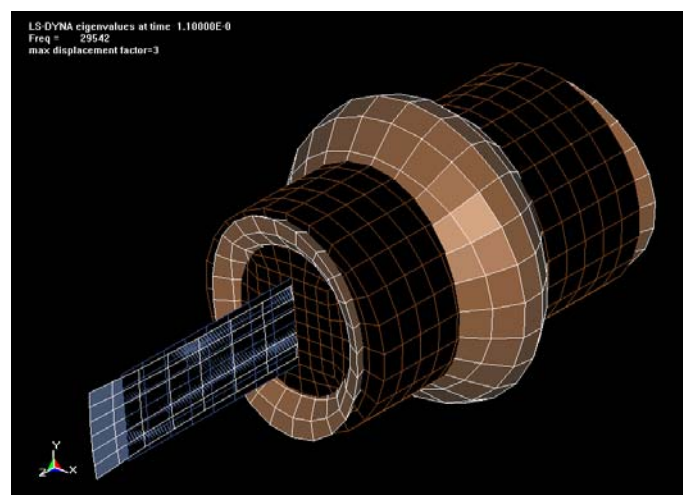
c.



d.



e.



f.

Figure 37. Mode shapes for a fundamental frequency.

2.3 Simplified Simulation

The full FE model runs for few hours on a single processor CPU. For parametric studies, this run time is considered to be long. A simplified methodology in which an FE model can run in few minutes is developed. This methodology requires that a set of simulations be run for each OBR configuration (see figure 1b, for example) with the discrete spring-mass model shown in figure 2, and extract the force exerted between the test item and the mitigator. The contact forces (F in figure 2) between the OBR and the mitigator could subsequently be used in a simplified FE model of the test item only. For a given contact force corresponding to a given OBR weight and configuration, an FE mesh of the OBR (test item) could be analyzed that requires a shorter run time. Any modification in the OBR content that may be required because of the addition of a new electronics package to be tested could easily be modeled in the simplified FE mesh of the OBR for a given force. To simulate the response of the OBR, the contact force is applied as an external force to the OBR to resist the momentum of the OBR. This methodology is applied to the current model and presented next.

For the test item used in figure 1b, the contact force between the mitigator and the OBR is presented in figure 38. This force is then applied as an external force to the OBR FE model (the only mesh is the OBR) for a given initial impact velocity. The acceleration data are collected from the simplified model and compared to full model in figure 39. One can observe that they are practically the same. The simplified model runs in less than a minute.

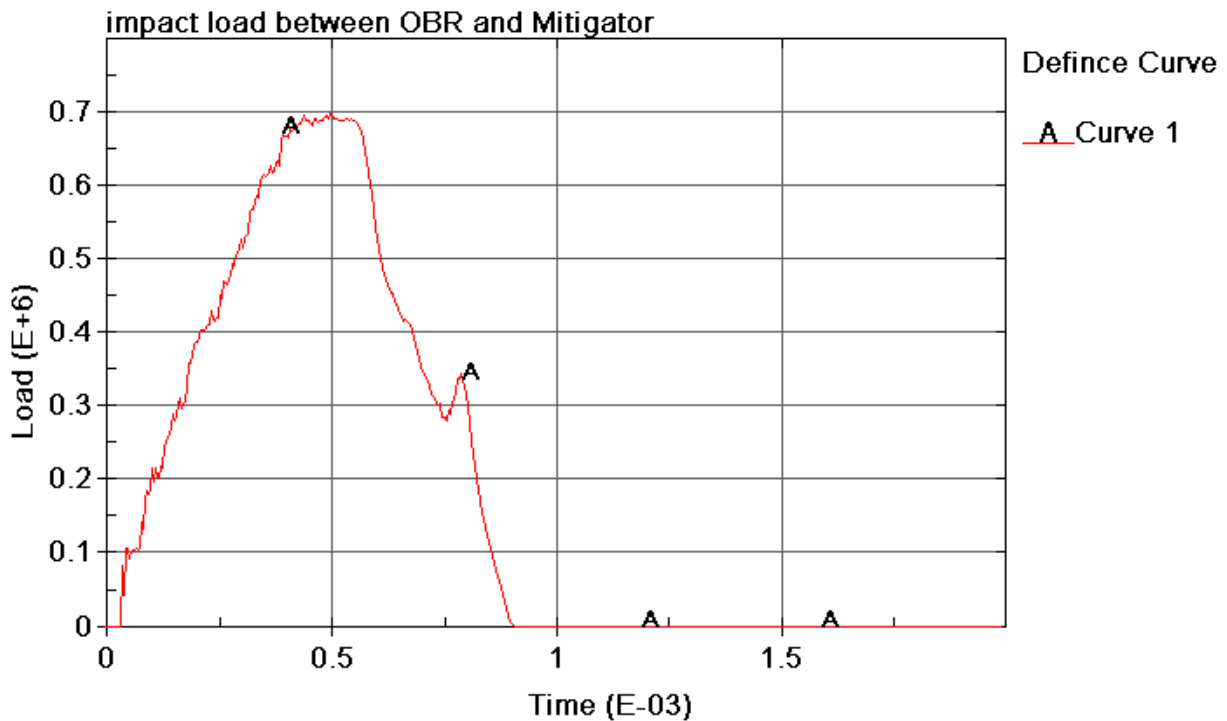


Figure 38. Contact force between the OBR and the mitigator.

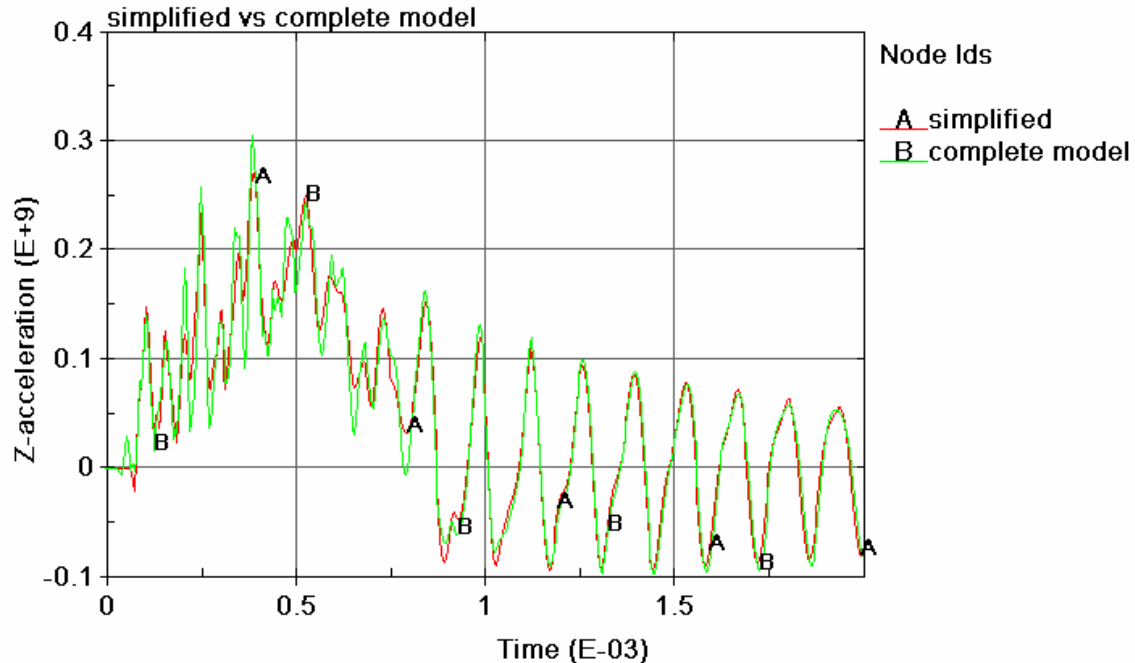


Figure 39. Acceleration data of the simplified and full model.

2.4 Conclusion

The sensitivity of FE model parameters affecting the dynamics of a test object launched in an air gun test is discussed in this part of the report. An LS-DYNA FE model previously developed to simulate the impact mitigation environment is used to investigate the sensitivity of FE model parameters. Previous study indicates the necessity of honeycomb material characterization under very high impact loading for effective modeling of the strain rate effects. The sensitivity study clearly indicates that the model is numerically stable and can aid in failure prediction if damping is added. A comparison of FE simulation responses with various damping options suggests that the mass proportional damping attenuates the low frequency vibration in the simulated response while the stiffness proportional damping attenuates the high frequency oscillations. The FE analysis also suggests that intermittent eigenvalue analyses during an impact simulation could be useful in identifying the dominant modes of vibration governing the dynamics of the test items and verifying the predictive capability of the FE model. The reasons that the FE model predicted high frequency content (above 14,000 Hz) that is not observed in the test could include (a) a lack of information for material characterization of the honeycomb mitigator under very high strain rate, or (b) lack of a proper material model for the beads which has significant damping at high frequencies.

An efficient procedure using a simplified decoupled model is proposed to simulate the response of a test item launched in an air gun test. In this approach, the contact force generated from the discrete analytical model is applied on a detailed FE mesh of the test item for a given impact velocity. The acceleration data obtained by this procedure compared well with those of the full

FE analysis. This model is programmed in a FORTRAN code that can produce results with only a few minutes of run time which are comparable to the FE and test results. This procedure can aid in the prediction of the failure of MEMS in the OBR with deformable FE model.

3. References

1. Lu, Wei-Yang; Hinnerichs, T. Crush of High Density Aluminum Honeycombs. *Proceedings of 2001 ASME International Mechanical Engineering Congress and Exposition*, AMD-Vol. 251, pp. 203–211, 2001.
2. Ashby, M.F.; Evans, A.G.; Hutchinson, J.W.; Fleck, N. A. *Metal Foams: A Design Guide*, University of Cambridge: Cambridge, 1998.
3. Reid, S.R.; Peng, C. Dynamic Uniaxial Crushing of Wood, *International Journal of Impact Engineering*, Vol. 19, Nos. 5–6, pp. 531–570, 1997.
4. Zhao, H.; Elnasri, I.; Abdennadher, S. An experimental study on the behavior under impact loading of metallic cellular materials, *International Journal of material Sciences*, Vol. 47, pp. 757–774, 2005.
5. Zhang, J.; Kikuchi, N.; Li, V.; Yee, A.; Nusholtz, G. Constitutive Modeling of Polymeric Foam Material Subjected to Dynamic Crash Loading, *International Journal of Impact Engineering*, Vol. 21, No. 5, pp. 369–386, 1998.
6. Chowdhury, M.; Tabiei, A. *Transient Response of Projectile in Gun Launch Simulation Using LS-DYNA Models*; ARL-TR-125; U.S. Army Research Laboratory: Aberdeen Proving Ground, MD, 2003.

Appendix A. Program I/O Files and FORTRAN Source Code

Input File

The input parameters necessary for the impact model are entered in an ASCII text file named “input.dat,” which needs to be located in the same directory as the program executable. A sample input file with brief description of the input parameters follows:

1.25	M1 - mass of OBR back
2.5	M2 - mass of OBR front
31.2	M3 - mass of MEM
2.0E6	K1 - OBR spring stiffness
83.566	V0 - OBR initial velocity
0.002	End time of analysis
1.0E-6	Time step for analysis
4.0E-6	Output time step
0.64	Compacting strain
82.74E3	Yield stress
4.060E6	Elastic modulus
650.0	Density of honeycomb
0.05	Radius of mitigator
0.038	Length of wedge part
0.219	Length of cylindrical part

Notes:

The input parameters must be in consistent units. The program does not check for unit consistency nor does it convert the input values to ensure consistency. The units used in the above input are kilogram, second, meter, Newton.

The program reads only the first input parameter from each line of the input file. Everything after the first parameter is treated as comments. However, the first parameter should have the appropriate value of the corresponding variable and be in the appropriate numeric format.

The input parameters should be entered in the exact order as shown in the example above. There should be no empty lines at the beginning of the input file.

Output Files

The program produces several output files:

output.dat – an ASCII file with all the output information in different columns. There are 12 columns having the values of current analysis time, displacement, velocity, and acceleration of masses M_1 , M_2 , and M_3 , current force value, and current plastic front location.

LS_POSTdis.dat – an ASCII file with the displacements of the three mass attachment points. This file is in LSTC LS-POST format.

LS_POSTvel.dat – an ASCII file with the velocities of the three mass attachment points. This file is in LSTC LS-POST format.

LS_POSTacc.dat – an ASCII file with the accelerations of the three mass attachment points. This file is in LSTC LS-POST format.

LS_POSTfor.dat – an ASCII file with the contact force between the mitigator and OBR (MEM). This file is in LSTC LS-POST format.

FORTRAN Source Code

The FORTRAN source code of the program implementing the formulation described in section “Model Formulation” follows below.

```

      program main
      double precision uml(3),un(3),upl(3),udn(3),uddn(3),xklu,
*      buff(10),cpl,xfront,dxfront,Force
c      Initialize
      xpi=3.1415926536
      open (10,file='input.dat')
      read(10,*)xM1
      read(10,*)xM2
      read(10,*)xM3
      read(10,*)xK1
      read(10,*)xV0
      curtime=0.
      read(10,*)endtime
      read(10,*)dt
      dt2=dt**2
      curout=0.
      read(10,*)dtout
      mcount=0
      read(10,*)epsc
      read(10,*)sigy
      read(10,*)Emod
      epsy=sigy/Emod
      read(10,*)rho0
      rhoym=rho0/(1.-epsc)
      rhoym=rho0/(1.-epsc)
      read(10,*)radius
      read(10,*)xLwed
      read(10,*)xLcyl
      close(10)
      xfront=0.
      area0=xpi*radius**2
      Force=0.
c      Time = 0
```

```

c   Displacement
    un(1)=0.
    un(2)=0.
    un(3)=0.
c   Velocity
    udn(1)=xV0
    udn(2)=xV0
    udn(3)=0.
c   Acceleration
    uddn(1)=0.
    uddn(2)=0.
    uddn(3)=0.
c   Displacement at -dt
    do i=1,3
        um1(i)=-dt*udn(i)
    end do
c   Define output
    open (10,file='output.dat')
c   End Initialization, Define Time Stepping Loop
c
c   Stop when acceleration of MEM gets zero
c   do while (uddn(3).gt.0.0)
c
c   Or stop at endtime
c
    do while (curtime.lt.endtime)
c   Write values for displacement, velocity and acceleration
    if (curtime.ge.(curout+dtout)) then
        curout=curtime
        write(10,10)curtime,(un(i),udn(i),uddn(i),i=1,3),Force,xfront
        mcount=mcount+1
    end if
c   Calculate mitigator force
    cpl=(udn(2)-udn(3))/epsc
    if (cpl.gt.0.) then
c   Plastic region grows
        dxfront=cpl*dt
        xfront=xfront+dxfront

```

```

if (xfront.lt.xLwed) then
  areac=area0*xfront/xLwed
else
  areac=area0
end if
  Force=sigy*areac
else
c   Elasicity only; unloading
  Force=Force+
*   area0*Emod*(udn(2)-udn(3))*dt/(xLwed+xLcyl+un(3)-un(2)-xfront)
end if
  if (Force.lt.0.) Force=0.
c   Get new displacement values
  xklu=xK1*(un(1)-un(2))
  up1(1)=2.*un(1)-um1(1)-dt2*xklu/xM1
  up1(2)=2.*un(2)-um1(2)+dt2*(xklu-Force)/xM2
  up1(3)=2.*un(3)-um1(3)+dt2*Force/xM3
  do i=1,3
c   Velocity and acceleration
    udn(i)=.5*(up1(i)-um1(i))/dt
    uddn(i)=(up1(i)-2.*un(i)+um1(i))/dt2
c   Shift displacements in matrix
    um1(i)=un(i)
    un(i)=up1(i)
  end do
c   Step forward in time
  curtime=curtime+dt
end do
c   Write LS-POST output files
  open (11,file='LS_POSTdis.dat')
  write(11,20)
  do i=1,3
  rewind(10)
  write (11,30)i,mcount
  do j=1,mcount
  read(10,*)curtime,(buff(k),k=1,10)
  write(11,40)curtime, buff(3*i-2)
  end do

```

```

write(11,50)
end do
close(11)
open (11,file='LS_POSTvel.dat')
write(11,120)
do i=1,3
rewind(10)
write (11,130)i,mcount
do j=1,mcount
read(10,*)curtime,(buff(k),k=1,10)
write(11,140)curtime, buff(3*i-1)
end do
write(11,50)
end do
close(11)
open (11,file='LS_POSTacc.dat')
write(11,220)
do i=1,3
rewind(10)
write (11,230)i,mcount
do j=1,mcount
read(10,*)curtime,(buff(k),k=1,10)
write(11,240)curtime, buff(3*i)
end do
write(11,50)
end do
close(11)
open (11,file='LS_POSTfor.dat')
write(11,320)
rewind(10)
write (11,330)mcount
do j=1,mcount
read(10,*)curtime,(buff(k),k=1,10)
write(11,340)curtime, buff(10)
end do
write(11,50)
close(11)
close(10)

```

```

10 format(11(E12.6,',' , '1X),E12.6)
20 format ('Curveplot',/'ARL GUN SIMULATION',/'Time',
*         /'Displacement',/'Mass')
30 format('Displ. of M',I1,' #pts=',I10)
40 format(E12.6,2X,E12.6)
50 format('endcurve')
120 format ('Curveplot',/'ARL GUN SIMULATION',/'Time',
*         /'Velocity',/'Mass')
130 format('Veloc. of M',I1,' #pts=',I10)
140 format(E12.6,2X,E12.6)
220 format ('Curveplot',/'ARL GUN SIMULATION',/'Time',
*         /'Acceleration',/'Mass')
230 format('Accel. of M',I1,' #pts=',I10)
240 format(E12.6,2X,E12.6)
320 format ('Curveplot',/'ARL GUN SIMULATION',/'Time',
*         /'Force',/'Mass')
330 format('Contact Force', ' #pts=',I10)
340 format(E12.6,2X,E12.6)
    stop
    end

```

<u>NO. OF COPIES</u>	<u>ORGANIZATION</u>
1 (PDF ONLY)	DEFENSE TECHNICAL INFORMATION CTR DTIC OCA 8725 JOHN J KINGMAN RD STE 0944 FORT BELVOIR VA 22060-6218
1	US ARMY RSRCH DEV & ENGRG CMD SYSTEMS OF SYSTEMS INTEGRATION AMSRD SS T 6000 6TH ST STE 100 FORT BELVOIR VA 22060-5608
1	INST FOR ADVNCD TCHNLGY THE UNIV OF TEXAS AT AUSTIN 3925 W BRAKER LN STE 400 AUSTIN TX 78759-5316
1	DIRECTOR US ARMY RESEARCH LAB IMNE ALC IMS 2800 POWDER MILL RD ADELPHI MD 20783-1197
1	DIRECTOR US ARMY RESEARCH LAB AMSRD ARL CI OK TL 2800 POWDER MILL RD ADELPHI MD 20783-1197
2	DIRECTOR US ARMY RESEARCH LAB AMSRD ARL CS OK T 2800 POWDER MILL RD ADELPHI MD 20783-1197
21	DIRECTOR US ARMY RSCH LABORATORY ATTN AMSRD ARL WM MB A FRYDMAN M CHOWDHURY 2800 POWDER MILL RD ADELPHI MD 20783-1197
1	DIRECTOR US ARMY RSCH LABORATORY ATTN AMSRD ARL SE DE R ATKINSON 2800 POWDER MILL RD ADELPHI MD 20783-1197
1	RD&E COMMAND SYSTEMS OF SYSTEMS INTEGRATION ATTN AMSRD SS T 6000 6TH STREET STE 100 FT BELVOIR VA 22060-5688

<u>NO. OF COPIES</u>	<u>ORGANIZATION</u>
1	LAWRENCE LIVERMORE NATL LABS ATTN MS9042 WEI-YANG LU PO BOX 808 L 125 LIVERMORE CA 94551-0969
5	LAWRENCE LIVERMORE NATL LABS ATTN R CHRISTENSEN S DETERESA F MAGNESS M FINGER MS 313 M MURPHY L 099 PO BOX 808 LIVERMORE CA 94550
1	SANDIA NATL LABS ATTN MS0847 T HINNERICHS PO BOX 969 ALBUQUERQUE NM 87123
3	DIR SANDIA NATL LABS APPLIED MECHANICS DEPT ATTN MS 9042 J HANDROCK Y R KAN J LAUFFER PO BOX 969 ALBUQUERQUE NM 87123
5	UNIV OF CINCINNATI AEROSPACE ENGINEERING DEPT ATTN PROF ALA TABIEI CINCINNATI OH 45221
1	CDR US ARMY ARDEC ATTN AMSTA AR CC COL JANKER PICATINNY ARSENAL NJ 07806-5000
6	CDR US ARMY ARDEC ATTN AMSTA AR CCH A F ALTAMURA M NICOLICH M PALATHINGUL R HOWELL A VELLA M YOUNG PICATINNY ARSENAL NJ 07806-5000
1	CDR US ARMY ARDEC ATTN AMSRD AAR AEM D VO PICATINNY ARSENAL NJ 07806-5000
5	CDR US ARMY ARDEC ATTN AMSTA AR CCH A L MANOLE S MUSALLI M LUCIANO E LOGSDEN T LOUZEIRO PICATINNY ARSENAL NJ 07806-5000
1	CDR US ARMY ARDEC ATTN AMSRD AAR AEM L R CARR PICATINNY ARSENAL NJ 07806-5000

<u>NO. OF</u> <u>COPIES</u>	<u>ORGANIZATION</u>
5	CDR US ARMY ARDEC ATTN AMSTA AR CCH B P DONADIA F DONLON P VALENTI C KNUTSON G EUSTICE PICATINNY ARSENAL NJ 07806-5000
4	CDR US ARMY ARDEC ATTN AMSTA AR CCH B K HENRY J MCNABOC R SAYER F CHANG PICATINNY ARSENAL NJ 07806-5000
2	CDR US ARMY ARDEC ATTN AMSTA AR CCH C H CHANIN S CHICO PICATINNY ARSENAL NJ 07806-5000
1	CDR US ARMY ARDEC ATTN AMSTA AR CCH P J LUTZ PICATINNY ARSENAL NJ 07806-5000
2	CDR US ARMY ARDEC ATTN AMSRD AAR AEM I D CONWAY ATTN AMSRD AAR AEW E(D) R SCHLENNER PICATINNY ARSENAL NJ 07806-5000
3	CDR US ARMY ARDEC ATTN AMSTA AR FSA A WARNASH B MACHAK M CHIEFA PICATINNY ARSENAL NJ 07806-5000
1	CDR US ARMY ARDEC ATTN AMSTA AR FSE PICATINNY ARSENAL NJ 07806-5000
1	CDR US ARMY ARDEC ATTN AMSTA AR FSF T C LIVECCHIA PICATINNY ARSENAL NJ 07806-5000
2	CDR US ARMY ARDEC ATTN AMSTA AR FSP G M SCHIKSNIS D CARLUCCI PICATINNY ARSENAL NJ 07806-5000
1	CDR US ARMY ARDEC ATTN AMSTA AR M D DEMELLA PICATINNY ARSENAL NJ 07806-5000
1	CDR US ARMY ARDEC ATTN AMSTA AR QAC T D RIGOGLIOSO PICATINNY ARSENAL NJ 07806-5000

<u>NO. OF</u> <u>COPIES</u>	<u>ORGANIZATION</u>
1	CDR US ARMY ARDEC ATTN AMSTA AR QAC T C J PAGE PICATINNY ARSENAL NJ 07806-5000
1	CDR US ARMY ARDEC ATTN AMSTA AR TD PICATINNY ARSENAL NJ 07806-5000
1	CDR US ARMY ARDEC ATTN AMSTA AR WEA J BRESCIA PICATINNY ARSENAL NJ 07806-5000
1	CDR US ARMY ARDEC ATTN AMSTA AR WEL F M GUERRIERE PICATINNY ARSENAL NJ 07806-5000
1	CDR US ARMY ARDEC PRODUCTION BASE MODERN ACTY ATTN AMSMC PBM K PICATINNY ARSENAL NJ 07806-5000
1	PM ARMS ATTN SFAE GCSS ARMS BLDG 171 PICATINNY ARSENAL NJ 07806-5000
1	PM MAS ATTN SFAE AMO MAS PICATINNY ARSENAL NJ 07806-5000
1	PM MAS ATTN SFAE AMO MAS CHIEF ENGINEER PICATINNY ARSENAL NJ 07806-5000
1	PM MAS ATTN SFAE AMO MAS PS PICATINNY ARSENAL NJ 07806-5000
1	PM MAS ATTN SFAE AMO MAS LC PICATINNY ARSENAL NJ 07806-5000
1	PM MAS ATTN SFAE AMO MAS MC PICATINNY ARSENAL NJ 07806-5000
1	CDR US ARMY TACOM PM ABRAMS ATTN SFAE ASM AB 6501 ELEVEN MILE RD WARREN MI 48397-5000

NO. OF
COPIES ORGANIZATION

1 CDR US ARMY TACOM
 ATTN AMSTA SF
 WARREN MI 48397-5000

1 CDR US ARMY TACOM
 PM BFVS
 ATTN SFAE GCSS W BV
 6501 ELEVEN MILE RD
 WARREN MI 48397-5000

1 CDR US ARMY TACOM
 CHIEF ABRAMS TESTING
 ATTN SFAE GCSS W AB QT T KRASKIEWICZ
 6501 ELEVEN MILE RD
 WARREN MI 48397-5000

1 DIR AIR FORCE RSCH LAB
 ATTN MLLMD D MIRACLE
 2230 TENTH ST
 WRIGHT PATTERSON AFB OH 45433-7817

1 OFC OF NAVAL RESEARCH
 ATTN J CHRISTODOULOU
 ONR CODE 332
 800 N QUINCY ST
 ARLINGTON VA 22217-5600

1 CDR WATERVLIET ARSENAL
 ATTN SMCWV QAE Q B VANINA
 BLDG 44
 WATERVLIET NY 12189-4050

1 TNG DOC & CBT DEV
 ATTN ATZK TDD IRSA A POMEY
 FT KNOX KY 40121

2 HQ IOC TANK
 AMMUNITION TEAM
 ATTN AMSIO SMT R CRAWFORD
 W HARRIS
 ROCK ISLAND IL 61299-6000

1 CDR US ARMY AMCOM
 AVIATION APPLIED TECH DIR
 ATTN J SCHUCK
 FT EUSTIS VA 23604-5577

1 NAVAL SURFACE WARFARE CTR
 ATTN DAHLGREN DIV CODE G06
 DAHLGREN VA 22448

NO. OF
COPIES ORGANIZATION

4 CDR US ARMY TACOM
 ATTN AMSTA TR R R MCCLELLAND
 D THOMAS J BENNETT
 D HANSEN
 WARREN MI 48397-5000

1 CDR US ARMY TACOM
 ATTN AMSTA JSK A SCHUMACHER
 WARREN MI 48397-5000

2 CDR US ARMY TACOM
 ATTN AMSTA TR R S GOODMAN
 D TEMPLETON MS-263
 WARREN MI 48397-5000

3 CDR US ARMY TACOM
 ATTN AMSTA TR D D OSTBERG
 L HINOJOSA B RAJU
 WARREN MI 48397-5000

2 CDR US ARMY TACOM
 ATTN AMSTA CS SF H HUTCHINSON
 F SCHWARZ
 WARREN MI 48397-5000

10 BENET LABORATORIES
 ATTN AMSTA AR CCB R FISCELLA
 M SOJA E KATHE M SCAVULO
 G SPENCER P WHEELER
 S KRUPSKI J VASILAKIS
 G FRIAR R HASENBEIN
 WATERVLIET NY 12189-4050

4 BENET LABORATORIES
 ATTN AMSTA CCB R S SOPOK
 E HYLAND D CRAYON
 R DILLON
 WATERVLIET NY 12189-4050

2 US ARMY CORPS OF ENGINEERS
 ATTN CERD C T LIU
 CEW ET T TAN
 20 MASSACHUSETTS AVE NW
 WASHINGTON DC 20314

1 US ARMY COLD REGIONS
 RSCH & ENGRNG LAB
 ATTN P DUTTA
 72 LYME RD
 HANOVER NH 03755

1 USA SBCCOM PM SOLDIER SPT
 ATTN AMSSB PM RSS A J CONNORS
 KANSAS ST
 NATICK MA 01760-5057

<u>NO. OF COPIES</u>	<u>ORGANIZATION</u>
2	USA SBCCOM MATERIAL SCIENCE TEAM ATTN AMSSB RSS J HERBERT M SENNETT KANSAS ST NATICK MA 01760-5057
2	OFC OF NAVAL RESEARCH ATTN D SIEGEL CODE 351 J KELLY 800 N QUINCY ST ARLINGTON VA 22217-5660
1	NAVAL SURFACE WARFARE CTR TECH LIBRARY CODE 323 17320 DAHLGREN RD DAHLGREN VA 22448
1	NAVAL SURFACE WARFARE CTR CRANE DIVISION ATTN M JOHNSON CODE 20H4 LOUISVILLE KY 40214-5245
2	NAVAL SURFACE WARFARE CTR ATTN U SORATHIA C WILLIAMS CD 6551 9500 MACARTHUR BLVD WEST BETHESDA MD 20817-5700
2	CDR NAVAL SURFACE WARFARE CTR CARDEROCK DIVISION ATTN R PETERSON CODE 2020 M CRITCHFIELD CODE 1730 BETHESDA MD 20084
1	NAVAL SURFACE WARFARE CTR CARDEROCK DIVISION ATTN R CRANE CODE 6553 9500 MACARTHUR BLVD WEST BETHESDA MD 20817-5700
3	DIR US ARMY NATL GROUND INTEL CTR ATTN D LEITER MS 404 M HOLTUS MS 301 M WOLFE MS 307 2055 BOULDERS RD CHARLOTTESVILLE VA 22911-8318
2	DIR US ARMY NATL GROUND INTEL CTR ATTN S MINGLEDORF MS 504 J GASTON MS 301 2055 BOULDERS RD CHARLOTTESVILLE VA 22911-8318

<u>NO. OF COPIES</u>	<u>ORGANIZATION</u>
3	DIR US ARMY NATL GROUND INTEL CTR ATTN IANG TMT 2055 BOULDERS RD CHARLOTTESVILLE VA 22911-8318
1	NAVAL SEA SYSTEMS CMD ATTN D LIESE 1333 ISAAC HULL AVE SE 1100 WASHINGTON DC 20376-1100
4	US ARMY SBCCOM SOLDIER SYSTEMS CTR BALLISTICS TEAM ATTN J WARD W ZUKAS J SONG P CUNNIFF KANSAS ST NATICK MA 01760-5019
1	US ARMY SBCCOM SOLDIER SYSTEMS CTR MARINE CORPS TEAM ATTN J MACKIEWICZ KANSAS ST NATICK MA 01760-5019
2	US ARMY SBCCOM SOLDIER SYSTEMS CTR ATTN AMSSB RCP SS W NYKVIST S BEAUDOIN KANSAS ST NATICK MA 01760-5019
7	US ARMY RSCH OFC ATTN A CROWSON H EVERITT J PRATER G ANDERSON D STEPP D KISEROW J CHANG PO BOX 12211 RSCH TRIANGLE PARK NC 27709-2211
1	AFRL MLBC 2941 P ST RM 136 WRIGHT PATTERSON AFB OH 45433-7750
1	AFRL/MLMP ATTN R THOMSON 2977 HOBSON WAY BLDG 653 RM 215 WRIGHT PATTERSON AFB OH 45433-7739
2	AFRL ATTN F ABRAMS J BROWN BLDG 653 2977 P ST STE 6 WRIGHT PATTERSON AFB OH 45433-7739

<u>NO. OF COPIES</u>	<u>ORGANIZATION</u>
1	AFRL MLS OL ATTN L COULTER 5851 F AVE BLDG 849 RM AD1A HILL AFB UT 84056-5713
4	NAVAL SURFACE WARFARE CTR ATTN J FRANCIS CODE T08 D WILSON CODE B56 R D COOPER CODE G32 J FRAYSSE CODE G33 DAHLGREN VA 22448
2	NAVAL SURFACE WARFARE CTR ATTN L DE SIMONE CODE G33 R HUBBARD CODE G33 DAHLGREN VA 22448
1	DIR LOS ALAMOS NATIONAL LAB FL ADDESSIO T 3 MS 5000 PO BOX 1633 LOS ALAMOS NM 87545
1	OSD JOINT CCD TEST FORCE OSD JCCD ATTN R WILLIAMS 3909 HALLS FERRY RD VICKSBURG MS 29180-6199
2	DARPA ATTN S WAX L CHRISTODOULOU 3701 N FAIRFAX DR ARLINGTON VA 22203-1714
2	SERDP PROGRAM OFC PM P2 ATTN B SMITH 901 N STUART ST STE 303 ARLINGTON VA 22203
3	OAK RIDGE NATL LABORATORY ATTN R M DAVIS C EBERLE MS 8048 C D WARREN MS 8039 PO BOX 2008 OAK RIDGE TN 37831-6195
4	NIST ATTN M VANLANDINGHAM MS 8621 J CHIN MS 8621 J MARTIN MS 8621 D DUTHINH MS 8611 100 BUREAU DR GAITHERSBURG MD 20899

<u>NO. OF COPIES</u>	<u>ORGANIZATION</u>
1	HYDROGEOLOGIC INC SERDP ESTCP SPT OFC ATTN S WALSH 1155 HERNDON PKWY STE 900 HERNDON VA 20170
2	US ARMY RSRCH LAB NASA VEHICLE TECHNOLOGY CENTER ATTN AMSRL VS W ELBER MS 266 F BARTLETT JR MS 266 HAMPTON VA 23681-0001
1	NASA LANGLEY RSCH CTR ATTN G FARLEY MS 266 HAMPTON VA 23661-3400
1	FHWA ATTN E MUNLEY 6300 GEORGETOWN PIKE MCLEAN VA 22101
1	USDOT FEDERAL RAILRD ATTN M FATEH RDV 31 WASHINGTON DC 20590
3	CYTEC FIBERITE ATTN R DUNNE D KOHLI R MAYHEW 1300 REVOLUTION ST HAVRE DE GRACE MD 21078
1	3TEX CORPORATION ATTN A BOGDANOVICH 109 MACKENAN DR CARY NC 27511
1	DIR DEFENSE INTEL AGENCY ATTN TA 5 K CRELLING WASHINGTON DC 20310
1	COMPOSITE MATERIALS INC ATTN D SHORTT 19105 63 AVE NE PO BOX 25 ARLINGTON WA 98223
1	JPS GLASS ATTN L CARTER PO BOX 260 SLATER RD SLATER SC 29683

<u>NO. OF</u>	<u>ORGANIZATION</u>
<u>COPIES</u>	
1	COMPOSITE MATERIALS INC ATTN R HOLLAND 11 JEWEL CT ORINDA CA 94563
1	SIMULA ATTN R HUYETT 10016 S 51ST ST PHOENIX AZ 85044
2	PROTECTION MATERIALS INC ATTN M MILLER F CRILLEY 14000 NW 58 CT MIAMI LAKES FL 33014
3	FOSTER MILLER M ROYLANCE W ZUKAS 195 BEAR HILL RD WALTHAM MA 02354-1196
1	ROM DEVELOPMENT CORP ATTN R O MEARA 136 SWINEBURNE ROW BRICK MARKET PLACE NEWPORT RI 02840
1	TEXTRON SYSTEMS ATTN M TREASURE 1449 MIDDLESEX ST LOWELL MA 01851
1	O GARA HESS & EISENHARDT ATTN M GILLESPIE 9113 LESAINTE DR FAIRFIELD OH 45014
1	MILLIKEN RSCH CORP ATTN M MACLEOD PO BOX 1926 SPARTANBURG SC 29303
1	CONNEAUGHT INDUSTRIES INC ATTN J SANTOS PO BOX 1425 COVENTRY RI 02816
1	ARMTEC DEFENSE PRODUCTS ATTN S DYER 85 901 AVE 53 PO BOX 848 COACHELLA CA 92236

<u>NO. OF</u>	<u>ORGANIZATION</u>
<u>COPIES</u>	
3	PACIFIC NORTHWEST LAB ATTN M SMITH G VAN ARSDALE R SHIPPELL PO BOX 999 RICHLAND WA 99352
5	ALLIANT TECHSYSTEMS INC ATTN C CANDLAND MN11 2830 C AAKHUS MN11 2830 B SEE MN11 2439 R DOHRN MN11 2830 D KAMDAR MN11 2830 5050 LINCOLN DR MINNEAPOLIS MN 55436-1097
3	ALLIANT TECHSYSTEMS INC ATTN N VLAHAKUS MN11 2145 S HAGLUND MN11 2439 M HISSONG MN11 2830 4700 NATHAN LANE N PLYMOUTH MN 55442-2512
1	R FIELDS 4680 OAKCREEK ST APT 206 ORLANDO FL 32835
1	APPLIED COMPOSITES ATTN W GRISCH 333 NORTH SIXTH ST ST CHARLES IL 60174
1	CUSTOM ANALYTICAL ENG SYS INC ATTN A ALEXANDER 13000 TENSOR LANE NE FLINTSTONE MD 21530
1	AAI CORPORATION ATTN DR N B MCNELLIS PO BOX 126 HUNT VALLEY MD 21030-0126
1	OFC DEPUTY UNDER SEC DEFNS ATTN J THOMPSON 1745 JEFFERSON DAVIS HWY CRYSTAL SQ 4 STE 501 ARLINGTON VA 22202
3	ALLIANT TECHSYSTEMS INC ATTN J CONDON E LYNAM J GERHARD WV01 16 STATE RT 956 PO BOX 210 ROCKET CENTER WV 26726-0210

NO. OF
COPIES ORGANIZATION

1 PROJECTILE TECHNOLOGY INC
515 GILES ST
HAVRE DE GRACE MD 21078

5 AEROJET GEN CORP
ATTN D PILLASCH T COULTER
C FLYNN D RUBAREZUL
M GREINER
1100 WEST HOLLYVALE ST
AZUSA CA 91702-0296

1 BRIGS COMPANY
ATTN J BACKOFEN
2668 PETERBOROUGH ST
HERNDON VA 22071-2443

1 ZERNOW TECHNICAL SERVICES
ATTN L ZERNOW
425 W BONITA AVE STE 208
SAN DIMAS CA 91773

2 GENERAL DYNAMICS OTS
FLINCHBAUGH DIV
ATTN K LINDE T LYNCH
PO BOX 127
RED LION PA 17356

1 GKN WESTLAND AEROSPACE
ATTN D OLDS
450 MURDOCK AVE
MERIDEN CT 06450-8324

5 SIKORSKY AIRCRAFT
ATTN G JACARUSO B KAY
T CARSTENSAN
S GARBO MS S330A
J ADELMANN
6900 MAIN ST
PO BOX 9729
STRATFORD CT 06497-9729

1 PRATT & WHITNEY
ATTN C WATSON
400 MAIN ST MS 114 37
EAST HARTFORD CT 06108

1 AEROSPACE CORP
ATTN G HAWKINS M4 945
2350 E EL SEGUNDO BLVD
EL SEGUNDO CA 90245

2 CYTEC FIBERITE
ATTN M LIN W WEB
1440 N KRAEMER BLVD
ANAHEIM CA 92806

NO. OF
COPIES ORGANIZATION

2 UDLP
ATTN G THOMAS M MACLEAN
PO BOX 58123
SANTA CLARA CA 95052

2 UDLP
ATTN R BRYNSVOLD
P JANKE MS 170
4800 EAST RIVER RD
MINNEAPOLIS MN 55421-1498

1 LOCKHEED MARTIN
SKUNK WORKS
ATTN D FORTNEY
1011 LOCKHEED WAY
PALMDALE CA 93599-2502

1 NORTHRUP GRUMMAN CORP
ELECTRONIC SENSORS & SYSTEMS DIV
ATTN E SCHOCH MS V 16
1745A W NURSERY RD
LINTHICUM MD 21090

1 GDLS DIVISION
ATTN D BARTLE
PO BOX 1901
WARREN MI 48090

1 GDLS
ATTN M PASIK
PO BOX 1800
STERLING HEIGHTS MI 48090-1800

1 GDLS
MUSKEGON OPERATIONS
ATTN M SOIMAR
76 GETTY ST
MUSKEGON MI 49442

1 GENERAL DYNAMICS
AMPHIBIOUS SYS
SURVIVABILITY LEAD
ATTN G WALKER
991 ANNAPOLIS WAY
WOODBIDGE VA 22191

5 INST FOR ADVANCED TECH
ATTN H FAIR I MCNAB
P SULLIVAN S BLESS
W REINECKE C PERSAD
4030-2 W BRAKER LN
AUSTIN TX 78759-5329

<u>NO. OF COPIES</u>	<u>ORGANIZATION</u>
1	ARROW TECH ASSO 1233 SHELBURNE RD STE D8 SOUTH BURLINGTON VT 05403-7700
1	R EICHELBERGER CONSULTANT 409 W CATHERINE ST BEL AIR MD 21014-3613
1	SAIC ATTN G CHRYSSOMALLIS 8500 NORMANDALE LAKE BLVD SUITE 1610 BLOOMINGTON MN 55437-3828
1	UCLA MANE DEPT ENGR IV ATTN H T HAHN LOS ANGELES CA 90024-1597
1	UMASS LOWELL PLASTICS DEPT ATTN N SCHOTT 1 UNIVERSITY AVE LOWELL MA 01854
1	IIT RESEARCH CENTER ATTN D ROSE 201 MILL ST ROME NY 13440-6916
1	MICHIGAN ST UNIV MSM DEPT ATTN R AVERILL 3515 EB EAST LANSING MI 48824-1226
1	PENN STATE UNIV ATTN C BAKIS 212 EARTH ENGR SCIENCES BLDG UNIVERSITY PARK PA 16802
1	PENN STATE UNIV ATTN R S ENGEL 245 HAMMOND BLDG UNIVERSITY PARK PA 16801
1	PURDUE UNIV SCHOOL OF AERO & ASTRO ATTN C T SUN W LAFAYETTE IN 47907-1282

<u>NO. OF COPIES</u>	<u>ORGANIZATION</u>
1	UNIV OF MAINE ADV STR & COMP LAB ATTN R LOPEZ ANIDO 5793 AEWB BLDG ORONO ME 04469-5793
1	JOHNS HOPKINS UNIV APPLIED PHYSICS LAB ATTN P WIENHOLD 11100 JOHNS HOPKINS RD LAUREL MD 20723-6099
1	UNIV OF DAYTON ATTN J M WHITNEY COLLEGE PARK AVE DAYTON OH 45469-0240
5	UNIV OF DELAWARE CTR FOR COMPOSITE MTRLS ATTN J GILLESPIE M SANTARE S YARLAGADDA S ADVANI D HEIDER 201 SPENCER LABORATORY NEWARK DE 19716
1	UNIV OF ILLINOIS AT URBANA CHAMPAIGN DEPT OF MATERIALS SCIENCE & ENGINEERING ATTN J ECONOMY 1304 WEST GREEN ST 115B URBANA IL 61801
1	MISSISSIPPI STATE UNIVERSITY DEPT OF AEROSPACE ENGRNG ATTN A J VIZZINI MISSISSIPPI STATE MS 39762
1	DREXEL UNIV ATTN A S D WANG 32ND & CHESTNUT ST PHILADELPHIA PA 19104
3	UNIV OF TEXAS AT AUSTIN CTR FOR ELECTROMECHANICS ATTN J PRICE A WALLS J KITZMILLER 10100 BURNET RD AUSTIN TX 78758-4497
1	VA POLYTECHNICAL INST & STATE UNIV DEPT OF ESM ATTN M W HYER BLACKSBURG VA 24061-0219

<u>NO. OF COPIES</u>	<u>ORGANIZATION</u>
1	SOUTHWEST RSCH INST ENGR & MATL SCIENCES DIV ATTN J RIEGEL 6220 CULEBRA RD PO DRAWER 28510 SAN ANTONIO TX 78228-0510
1	BATELLE NATICK OPERATIONS ATTN B HALPIN 313 SPEEN ST NATICK MA 01760
2	US MILITARY ACADEMY ATTN R D HAMPTON BLDG 752 MAHAN HALL WEST POINT NY 10996
	<u>ABERDEEN PROVING GROUND</u>
1	DIRECTOR US ARMY RSCH LABORATORY ATTN AMSRD ARL CI OK TECH LIB BLDG 4600
1	US AMSAA ATTN AMXSY TD P DIETZ BLDG 392
1	US ARMY ATC ATTN CSTE DTC AT AC I W C FRAZER BLDG 400
1	DIRECTOR US ARMY RSCH LABORATORY ATTN AMSRD ARL O AP EG M ADAMSON BLDG 245
1	DIRECTOR US ARMY RSCH LABORATORY ATTN AMSRD ARL SL BM D BELY BLDG 328
3	DIRECTOR US ARMY RSCH LABORATORY ATTN AMSRD ARL WM J SMITH J MCCAULEY M ZOLTOSKI BLDG 4600
1	DIRECTOR US ARMY RSCH LABORATORY ATTN AMSRD ARL WM B (CHIEF) BLDG 4600

<u>NO. OF COPIES</u>	<u>ORGANIZATION</u>
1	DIRECTOR US ARMY RSCH LABORATORY ATTN AMSRD ARL WM BA (CHIEF) BLDG 4600
2	DIRECTOR US ARMY RSCH LABORATORY ATTN AMSRD ARL WM BC P PLOSTINS J NEWILL BLDG 390
7	DIRECTOR US ARMY RSCH LABORATORY ATTN AMSRD ARL WM BD P CONROY B FORCH M LEADORE R LIEB B RICE R PESCE RODRIGUEZ A ZIELINSKI BLDG 4600
1	DIRECTOR US ARMY RSCH LABORATORY ATTN AMSRD ARL WM BD C LEVERITT BLDG 390
1	DIRECTOR US ARMY RSCH LABORATORY ATTN AMSRD ARL WM BF S WILKERSON BLDG 390
2	DIRECTOR US ARMY RSCH LABORATORY ATTN AMSRD ARL WM M S MCKNIGHT J MCCAULEY BLDG 4600
3	DIRECTOR US ARMY RSCH LABORATORY ATTN AMSRD ARL WM MA (CHIEF) L GHIORSE E WETZEL BLDG 4600
19	DIRECTOR US ARMY RSCH LABORATORY ATTN AMSRD ARL WM MC (CHIEF) R BOSSOLI E CHIN S CORNELISON D GRANVILLE B HART F PIERCE E RIGAS W SPURGEON BLDG 4600

NO. OF
COPIES ORGANIZATION

- 22 DIRECTOR
US ARMY RSCH LABORATORY
ATTN AMSRD ARL WM MB J BENDER
T BOGETTI J BROWN L BURTON
R CARTER K CHO W DEROSSET
G DEWING R DOWDING
W DRYSDALE R EMERSON
D GRAY D HOPKINS R KASTE
L KECSKES M MINNICINO
B POWERS D SNOHA J SOUTH
M STAKER J SWAB J TZENG
BLDG 4600
- 12 DIRECTOR
US ARMY RSCH LABORATORY
ATTN AMSRD ARL WM MD P DEHMER
B CHEESEMAN R DOOLEY
G GAZONAS S GHIORSE
M KLUSEWITZ J LASALVIA
J MONTGOMERY W ROY
J SANDS D SPAGNUOLO
S WALSH S WOLF
BLDG 4600
- 2 DIRECTOR
US ARMY RSCH LABORATORY
ATTN AMSRD ARL WM RP C SHOEMAKER
J BORNSTEIN
BLDG 1121
- 1 DIRECTOR
US ARMY RSCH LABORATORY
ATTN AMSRD ARL WM T B BURNS
BLDG 309
- 3 DIRECTOR
US ARMY RSCH LABORATORY
ATTN AMSRD ARL WM TA W GILLICH
C HOPPEL M ZOLTOSKI
BLDG 4600
- 5 DIRECTOR
US ARMY RSCH LABORATORY
ATTN AMSRD ARL WM TA T HAVEL
J RUNYEON M BURKINS
E HORWATH B GOOCH
BLDG 393
- 1 DIRECTOR
US ARMY RSCH LABORATORY
ATTN AMSRD ARL WM TB P BAKER
BLDG 390

NO. OF
COPIES ORGANIZATION

- 1 DIRECTOR
US ARMY RSCH LABORATORY
ATTN AMSRD ARL WM TC R COATES
BLDG 309
- 4 DIRECTOR
US ARMY RSCH LABORATORY
ATTN AMSRD ARL WM TD D DANDEKAR
M RAFTENBERG S SCHOENFELD
T WEERASOORIYA
BLDG 4600
- 1 DIRECTOR
US ARMY RSCH LABORATORY
ATTN AMSRD ARL WM TE (CHIEF)
BLDG 1116A

NO. OF
COPIES ORGANIZATION

FOREIGN ADDRESSES

1 LTD
R MARTIN
MERL
TAMWORTH RD
HERTFORD SG13 7DG
UK

1 CIVIL AVIATION
ADMINSTRATION
T GOTTESMAN
PO BOX 8
BEN GURION INTERNL AIRPORT
LOD 70150
ISRAEL

1 AEROSPATIALE
S ANDRE
A BTE CC RTE MD132
316 ROUTE DE BAYONNE
TOULOUSE 31060
FRANCE

1 DRA FORT HALSTEAD
P N JONES
SEVEN OAKS KENT TN 147BP
UK

1 SWISS FEDERAL ARMAMENTS
WKS
W LANZ
ALLMENDSTRASSE 86
3602 THUN
SWITZERLAND

1 DYNAMEC RESEARCH AB
AKE PERSSON
BOX 201
SE 151 23 SODERTALJE
SWEDEN

1 ISRAEL INST OF TECHNOLOGY
S BODNER
FACULTY OF MECHANICAL ENGR
HAIFA 3200
ISRAEL

1 DSTO
WEAPONS SYSTEMS DIVISION
N BURMAN RLLWS
SALISBURY
SOUTH AUSTRALIA 5108
AUSTRALIA

NO. OF
COPIES ORGANIZATION

1 DEF RES ESTABLISHMENT
VALCARTIER
A DUPUIS
2459 BOULEVARD PIE XI NORTH
VALCARTIER QUEBEC
CANADA
PO BOX 8800 COURCELETTE
GOA IRO QUEBEC
CANADA

1 INSTITUT FRANCO ALLEMAND
DE RECHERCHES DE SAINT LOUIS
DE M GIRAUD
RUE DU GENERAL
CASSAGNOU
BOITE POSTALE 34
F 68301 SAINT LOUIS CEDEX
FRANCE

1 LAB TECHNOLOGIES COMPOSTS
& POLYMERS
J MANSON
DMX LTC
CH 105 LAUSANNE EPFL-IMX
SWITZERLAND

1 TNO DEFENSE RESEARCH
R IJSSELSTEIN
ACCOUNT DIRECTOR
R&D ARMEE
PO BOX 6006
2600 JA DELFT
THE NETHERLANDS

1 FOA NATL DEFENSE RESEARCH
ESTAB
DIR DEPT OF WEAPONS &
PROTECTION
B JANZON
R HOLMLIN
S 172 90 STOCKHOLM
SWEDEN

1 DEFENSE TECH & PROC AGENCY
GROUND
I CREWTHER
GENERAL HERZOG HAUS
3602 THUN
SWITZERLAND

NO. OF
COPIES ORGANIZATION

- 1 MINISTRY OF DEFENCE
RAFAEL
ARMAMENT DEVELOPMENT
AUTH
M MAYSELESS
PO BOX 2250
HAIFA 31021
ISRAEL
- B HIRSCH
TACHKEMONY ST 6
NETAMUA 42611
ISRAEL
- 1 DEUTSCHE AEROSPACE AG
DYNAMICS SYSTEMS
M HELD
PO BOX 1340
D 86523 SCHROBENHAUSEN
GERMANY